Biogeosciences Discuss., 10, 7785–7830, 2013
www.biogeosciences-discuss.net/10/7785/2013/
doi:10.5194/bgd-10-7785-2013

Biogeosciences Discussions
Open Access

Modeling ocean circulation and biogeochemical variability in the Gulf of Mexico

Z. Xue[1], R. He[1], K. Fennel[2], W.-J. Cai[3], S. Lohrenz[4], and C. Hopkinson[5]

[1]Dept. of Marine, Earth & Atmospheric Sciences, North Carolina State University, Raleigh, NC, USA
[2]Dept. of Oceanography, Dalhousie University, Halifax, Canada
[3]School of Marine Science and Policy, University of Delaware, Newark, USA
[4]School for Marine Science and Technology, University of Massachusetts Dartmouth, New Bedford, MA, USA
[5]Department of Marine Sciences, University of Georgia, Athens, GA, USA

Received: 8 April 2013 – Accepted: 23 April 2013 – Published: 8 May 2013

Correspondence to: Z. Xue (zxue@ncsu.edu)

Published by Copernicus Publications on behalf of the European Geosciences Union.

Abstract

A three-dimensional coupled physical-biogeochemical model is applied to simulate and examine temporal and spatial variability of circulation and biogeochemical cycling in the Gulf of Mexico (GoM). The model is driven by realistic atmospheric forcing, open boundary conditions from a data assimilative global ocean circulation model, and observed freshwater and terrestrial nutrient input from major rivers. A 7 yr model hindcast (2004–2010) was performed, and validated against satellite observed sea surface height, surface chlorophyll, and in-situ observations including coastal sea-level, ocean temperature, salinity, and nutrient concentration. The model hindcast revealed clear seasonality in nutrient, phytoplankton and zooplankton distributions in the GoM. An Empirical Orthogonal Function analysis indicated a phase-locked pattern among nutrient, phytoplankton and zooplankton concentrations. The GoM shelf nutrient budget was also quantified, revealing that on an annual basis ~80 % of nutrient input was denitrified on the shelf and ~17 % was exported to the deep ocean.

1 Introduction

Continental shelves are known to play an important role in global biogeochemical cycling (e.g. Liu et al., 2010) and are generally considered as importers of fixed nitrogen from the open ocean (Seitzinger et al., 2006) and exporters of organic matter (Gattuso et al., 1998). The magnitude of organic and inorganic matter exchange between shelves and the open ocean is a key quantity, yet hard to determine empirically; thus estimates of these fluxes in coastal ocean/marginal seas are scarce.

The focus of this study is the Gulf of Mexico (GoM hereafter), which is the largest semi-enclosed marginal sea of the western Atlantic. Encompassing both eutrophic coastal waters and oligotrophic deep-ocean waters, it is a region with a very productive marine ecosystem (estimated at 150–300 g C m^{-2} yr^{-1}; Heileman and Rabalais, 2008), and an important global reservoir of biodiversity and biomass of fish, sea birds and

BGD
10, 7785–7830, 2013

marine mammals. The upper ocean circulation in the GoM is dominated by the energetic Loop Current (LC hereafter), which is part of the North Atlantic western boundary current system. Large anticyclonic eddies aperiodically pinch off from the LC with an interval ranging from 3 to 17 months (Sturges and Leben, 2000). Associated with the LC and LC eddies, are many smaller cyclonic and anticyclonic eddies. Confluence of along-shelf currents introduced by local wind stress and wind stress curl, together with interactions between eddies and shelf/slope circulation, can effectively transport high-chlorophyll shelf waters into the deep GoM (e.g., Muller-Karger et al., 1991; Toner et al., 2003; Zavala-Hidalgo et al., 2003). These transport processes therefore play a crucial role in changing temporal and spatial distributions of biogeochemical properties in the GoM, and subsequently the regional marine ecosystem dynamics.

Previous marine biogeochemical studies in the Gulf have been mainly based on satellite sea surface temperature and ocean color (surface chlorophyll) observations. Turbid and nutrient rich freshwater from major rivers and the associated high chlorophyll coastal waters have a strong impact on the coastal ocean color variability in the GoM (Muller-Karger et al., 1991; Gilbes et al., 1996; Jolliff et al., 2003; Toner et al., 2003; Martinez-Lopez and Zavala-Hidalgo, 2009; Nababan et al., 2011), especially in regions surrounding the Mississippi River delta, the shelf break off Veracruz, and the Bay of Campeche. Analyses of Gulf-wide, long-term satellite SST and ocean color data provide evidence that Gulf waters have two characteristic states: (1) a winter mixing period characterized by annual maxima of surface pigment concentration, and (2) a thermally stratified period characterized by the annual minimum of surface pigment concentration (Jolliff et al., 2008). One major limitation of satellite data is that they are insufficient to determine marine ecosystem variations in the water column, and whether the spatial and temporal variability in surface pigment (e.g., chlorophyll) is caused by local biological effects or by 3-dimensional ocean advection across large gradients. Because of the presence of relatively high concentrations of Colored Dissolved Organic Matter (CDOM), standard satellite data processing algorithms also tend to overestimate

BGD
10, 7785–7830, 2013

chlorophyll concentrations in the coastal regions (Nababan et al., 2011, also see observation/model data comparison in Sect. 3).

Ever-increasing human activities, such as shoreline development, changes in land use practices, and the resulting increases in pollutant and nutrient/carbon input continue to threaten the well-being of marine ecosystems in the GoM. Notable examples are coastal eutrophication, recurring hypoxia, a.k.a. the "Dead Zone" (e.g., Rabalais et al., 2002), and coastal ocean acidification (Cai et al., 2011) on the Louisiana-Texas shelf (LATEX hereafter). The Mississippi/Atchafalaya river system is the largest fluvial source in the GoM and delivers 1.5 million ton yr^{-1} nitrogen into the LATEX shelf. This nitrogen load has tripled from the 1970 to 1990s (Goolsby et al., 2001). The primary production and CO_2 uptake in the river plume has been found to be significantly correlated with increased inorganic nitrogen flux (e.g., Lohrenz et al., 1997; Guo et al., 2012). A classic explanation for the hypoxia on the LATEX shelf is that the nutrient-enhanced phytoplankton growth results in the delivery of enormous amounts of organic matter to bottom waters on the shelf. This organic matter is then respired microbially in the bottom water, drawing down the oxygen concentration and subsequently producing hypoxic conditions. Recent studies have shown that several other factors are also important in the formation of hypoxia (see Bianchi et al., 2010 for a detailed review). For example, Lehrter et al. (2009) reported that shelf-wide primary production was not significantly related to nutrient loading. Wiseman et al. (1997), CENR (2000), and Fennel et al. (2013) provide evidence that the physical-controlled stratification is an important process regulating hypoxia formation below the pycnocline. DiMarco et al. (2010) pointed out that spatial variability of dissolved oxygen concentration is closely linked to local topographic features. These recent ideas urge more comprehensive studies of physical and biogeochemical processes affecting the GoM marine ecosystem.

Progress in ocean modeling has also made it possible to apply coupled physical-biogeochemical models to realistically simulate and characterize marine ecosystem variations, and piece out complex physical and biogeochemical interactions (e.g., Walsh et al., 1989). More recently, Fennel et al. (2011) successfully reproduced many

BGD
10, 7785–7830, 2013

features of observed nutrient and phytoplankton dynamics on the LATEX shelf covering the period of 1990–2004. Model results indicate a positive correlation between primary production (phytoplankton biomass) and nitrogen loading. However, simulated phytoplankton growth rate was not correlated with nitrogen loading, suggesting that the accumulation of biomass may be controlled by loss processes (e.g. vertical sinking, mortality, grazing by zooplankton) as well. Fennel et al. (2013) further incorporated dissolved oxygen concentration into the coupled model and results supported the view that simulated hypoxia size is very sensitive to the parameterization of sediment oxygen consumption and vertical stratification.

In this study we present a coupled physical-biogeochemical modeling study of ocean circulation and biochemical cycling for the entire GoM. Complementary to the Fennel et al. (2011) study, our work is aimed at achieving an improved understanding of marine ecosystem variations and their relations with 3-dimensional ocean circulation in a gulf-wide context. Our specific objectives were to (1) investigate temporal and spatial variability of ocean circulation and marine ecosystem dynamics in the GoM, and (2) to quantify the nitrogen budget on the GoM shelf.

2 Methods

2.1 Physical model

The circulation hindcast model was implemented based on the Regional Ocean Modeling System (ROMS, Haidvogel et al. 2008; Shchepetkin and McWilliams, 2005). The model domain (Fig. 1) encompasses the entire Gulf of Mexico and South Atlantic Bight, hereafter SABGOM ROMS. Details of this model implementation are given in Hyun and He (2010). Briefly, the model has a horizontal resolution of 5 km. Vertically, there are 36 terrain-following layers weighted to better resolve surface and bottom boundary layers. For open boundary conditions, SABGOM ROMS is one-way nested inside the 1/12° data assimilative North Atlantic Hybrid Coordinate Ocean Model (HYCOM/NCODA,

BGD
10, 7785–7830, 2013

Chassignet et al., 2003). Open boundary conditions of water mass and baroclinic velocity were specified following the method of Marchesiello et al. (2001), whereby Orlanski-type radiation conditions were used in conjunction with relaxation to HyCOM/NCODA solutions. Free surface and depth-averaged velocity boundary conditions were specified using the method of Flather (1976) with the external subtidal information defined by HyCOM/NCODA plus eight tidal constituents (Q1, O1, P1, K1, N2, M2, S2, K2) derived from OTIS regional tidal solution (Egbert and Erofeeva, 2002). For both meteorological momentum and buoyancy forcing, we utilized 3-hourly, 32 km horizontal resolution North American Regional Reanalysis (NARR, www.cdc.noaa.gov). The Mellor and Yamada (1982) closure scheme was applied to compute the vertical turbulent mixing, as well as the quadratic drag formulation for the bottom friction specification.

2.2 Biogeochemical model

The SABGOM ROMS ocean circulation model is coupled with a marine biogeochemical model described in Fennel et al. (2006, 2008, 2011). While this biogeochemical model is capable of simulating phosphate limitation and the inorganic carbon processes in addition to nitrogen cycling, we focused on the nitrogen cycle first in this work. Omission of phosphate limitation is justified by results of earlier studies (e.g., Rabalais et al., 2002) that have shown that the primary production on the LATEX shelf is typically nitrogen-limited during the low discharge season, and that dissolved $NO_x : PO_4$ ratios are often higher than the 16 : 1 "Redfield Ratio" (Lohrenz et al., 2008, 1997, 1999). An understanding of the role of phosphate and how its rapid recycling affects regional marine ecosystem processes warrants more detailed study (e.g., Laurent et al., 2012 for the LATEX shelf). However, here we focus on nitrogen and will report on the role of P in a future correspondence.

The nitrogen cycling model under our consideration has seven state variables: two species of dissolved inorganic nitrogen (DIN hereafter): nitrate, (NO_3) and ammonium (NH_4), one functional phytoplankton group, chlorophyll as a separate state variable to

BGD
10, 7785–7830, 2013

allow for photoacclimation, one functional zooplankton group, and two pools of detritus representing large, fast-sinking particles, and suspended, small particles.

Freshwater and nitrogen input from 63 major rivers (38 in the United States, 23 in Mexico, and 2 in Cuba) along the Gulf coast and South Atlantic Bight were included in the coupled model simulation. For rivers located inside the United States, daily riverine fresh water discharge and inorganic nitrogen flux values were retrieved from the US Geological Survey river gauges (e.g. Aulenbach et al., 2007). Such riverine data were not available for Mexican and Cuban rivers however. Instead we utilized the long-term estimation or climatological means developed by Milliman and Farnsworth (2011), Fluentes-Yaco et al. (2001), and Nixon (1996). For the Mississippi and Atchafalaya Rivers in particular, we also considered riverine particulate organic nitrogen input, which was determined as the difference between Kjeldahl nitrogen and ammonium (Fennel et al., 2011). The particulate organic nitrogen flux for other rivers was assigned a small, positive value as no continuous Kjeldahl nitrogen observation was available.

Similar to the LATEX model simulation reported by Fennel et al. (2011), we specified SABGOM initial and boundary conditions of NO_3 using World Ocean Atlas data (Garcia et al., 2010). Other variables (NH_4, phytoplankton, chlorophyll, zooplankton, small and large particles) were initialized with small, positive values over the entire domain. Biogeochemical model parameters (i.e., phytoplankton growth/loss rates, remineralization and light attenuation) were chosen as those used in Fennel et al. (2011).

We performed a 7 yr (1 January 2004–31 December 2010) regional ocean circulation and marine ecosystem hindcast. The first year was used to spin up the biogeochemical model. Analyses described in the following sections focus on the next 6 yr period between 1 January 2005 and 31 December 2010.

One of the analyses to be discussed later in the text involves quantifying along-shelf and cross-shelf exchange of water and nutrients. To do that, we decomposed the model simulated velocity field into along- and across- 50 m isobath directions, then the cross-shelf and along-shelf nutrient flux were calculated according to the equation below:

BGD
10, 7785–7830, 2013

$$E_h = \int_{-50}^{0} U_h(z) \times N(z) \cdot \mathrm{d}z \quad \text{where} \quad U_h = \mathrm{proj}_{\_\nabla h} U \tag{1}$$

$$E_t = \int_{-50}^{0} U_t(z) \times N(z) \cdot \mathrm{d}z \quad \text{where} \quad U_t = \mathrm{proj}_{\_\nabla t} U \tag{2}$$

Here E_h and E_t are the nutrient transport fluxes (unit: mmol N s^{-1} m^{-1}) cross and along isobaths, respectively, U_h and U_t are the normal and tangential components of the velocity cross isobath (unit: m s^{-1}), respectively, N is the DIN concentration at a given depth (unit: mmol N m^{-3}), and Z is water depth (unit: m).

3 Model-data comparisons

Model-simulated physical and biogeochemical variables were validated against extensive satellite and in-situ observations (see Figs. 1 and 2 for positions of coastal sea level stations, and ship surveys). Hourly coastal sea level observations were obtained from 13 tidal gauges operated by the NOAA National Ocean Service/Center for Operational Oceanographic Products and Services (NOS/CO-OPS). We were especially interested in the model skill in resolving subtidal circulation processes because they dominate material property transport in the ocean. As such, a 36 h low pass filter was applied to both observed and modeled sea level time series to facilitate comparisons. An example of this can be seen in Fig. 3, which shows the comparisons between observed and modeled subtidal sea-levels in 2008 at Charleston, Fernandina Beach, Galveston, and Corpus Christi. At all these locations, the modeled sea level time series track their observational counterparts reasonably well. Both the seasonal trend and synoptic storm

BGD
10, 7785–7830, 2013

surge events (as results of hurricanes) are well reproduced. A more robust statistical assessment of the model skill over the entire 7 yr hindcast period is shown in the form of a Taylor diagram (Fig. 4; Taylor, 2001), where correlation coefficients, centered root mean square difference (RMSD) between observed and simulated subtidal sea-level, and their normalized standard deviations are all present in a single plot. At most of the 13 coastal stations mentioned above, the correlation coefficients between simulated and observed sea level range between 0.5 and 0.9, and the simulated sea-levels are within one standard deviation of the observed values.

In a Gulf-wide spatial context, we compared eddy kinetic energy (EKE hereafter) derived from satellite altimetry observations (AVISO Sea surface height) with model-simulated EKE. Reasonably good agreement was found between the satellite- and model-derived multi-year mean (2004–2010) EKE, an indication that the model is capable of reproducing Gulf-wide sea level and associated circulation and EKE distributions. It is not surprising to see that high EKE values were associated with the LC and its adjacent eddies in the GoM while the shelf regions (e.g. west Florida shelf, LATEX shelf) generally had low EKE.

We also took advantage of extensive in-situ observations (shipboard CTD casts and Niskin bottle samplings) collected during research cruises in the northern GoM spanning over the period of 2005–2010 (Data were collected from different sources, including the Environmental Protection Agency (Lehrter et al., 2009, 2012; Lohrenz et al., 2008; Cai et al., 2011; Huang et al., 2012); Louisiana Universities Marine Consortium (Rabalais et al., 2007); Mechanisms Controlling Hypoxia (MCH) Project; Southeast Monitoring and Assessment Program (SEAMAP), the NSF-funded GulfCarbon Project and Mississippi-Atchafalaya-Gulf of Mexico-Mixing Experiment (MMAGMIX)). Together, there are more than 8000 surface observations of water temperature, salinity, NO_3, NH_4, chlorophyll concentrations. To avoid the scale mismatch between in-situ point measurements and our 5 km model grid resolution, we followed the approach used in Fennel et al. (2011), and divided the northern Gulf area into 3 sub-regions (i.e. Delta, Intermediate, and Far-field, see Fig. 2). Observed and modeled (both are

BGD
10, 7785–7830, 2013

surface values unless otherwise stated) variables that fell into each sub-region were spatially averaged. The resulting time series comparisons were used to evaluate the model's skill in predicting each state variable under consideration. Figs. 6 and 7 show the comparisons between observed and simulated sea surface salinity (Fig. 6a), surface temperature (Fig. 6b), NO_3 (Fig. 7a), and chlorophyll (Fig. 7b). For chlorophyll, we also acquired Moderate Resolution Imaging Spectroradiometer (MODIS hereafter) satellite-derived monthly mean time series for the comparison in each of the three sub-regions. The model reproduced both seasonal and interannual variations of salinity, temperature, NO_3, and chlorophyll reasonably well. Simulated values generally fell within the 1 standard deviation range of corresponding observations. Surface temperature and salinity in all three sub-regions were characterized by clear seasonal cycles. We note that the model under-predicted a sharp salinity drop in spring-summer 2008, which was induced by the Mississippi River flooding during that year (White et al., 2009; also see freshwater discharge time series in Fig. 9a). This was likely due to small-scale variability in the Mississippi/Atchafalaya river plume structure that was not fully resolved by our 5 km resolution model.

Seasonal patterns of NO_3 and chlorophyll were similar. In general, these variables peaked in late spring-early summer (April–July) when riverine discharge was highest. The influence of river discharge and nutrient input on regional hydrography decreased rapidly with increasing distance from the delta. It was encouraging to see that model-simulated surface chlorophyll fields were in general agreement with those observed in situ (Fig. 7b). Surface chlorophyll observed by MODIS exhibited similar temporal variations, but generally overestimated the concentrations measured in situ. This was not surprising because MODIS estimates of chlorophyll were likely influenced by other optical constituents including suspended sediment and CDOM (e.g., Nababan et al., 2011). Nevertheless, MODIS imagery provided valuable information about the spatial distribution of surface chlorophyll, allowing the examination of model skill over the entire Gulf, as can been seen for the comparison of seasonal means of observed and simulated surface chlorophyll fields in the GoM (Fig. 8). These means were calculated

BGD
10, 7785–7830, 2013

by averaging MODIS-derived and model-simulated chlorophyll, respectively over a 6 yr period (2005–2010). The spatial correlation coefficients between the two were 0.60, 0.65, 0.53 and 0.45 for spring, summer, fall, and winter, respectively, suggesting that the model has intrinsic capability to reproduce the temporal and spatial variations of surface chlorophyll. Both MODIS data and model simulation show that high chlorophyll concentrations were present in coastal areas adjacent to major rivers, such as the LATEX shelf, the Bay of Campeche and Campeche Bank. The chlorophyll content was much lower in the deep ocean. In general, the surface chlorophyll concentration was higher in winter and spring than in summer and fall.

In summary, all the above-mentioned comparisons (Figs. 3–8) indicate that our coupled physical-biogeochemical model is capable of resolving the main spatiotemporal variations of circulation and biogeochemical variables in the GoM, providing confidence in our approach to use the 7 yr hindcast to further characterize the temporal and spatial variability of physical and biogeochemical dynamics over the entire Gulf.

4 Results and discussion

4.1 Nutrient, phytoplankton, and zooplankton dynamics

The Mississippi/Atchafalaya river system provides the majority of the nutrient loading on the LATEX shelf (Walsh et al., 1989; Turner and Rabalais, 1999). In our 7 yr simulation, we found riverine nutrient input on the LATEX shelf accounts for ~ 80 % of the total nitrogen loading in GoM (Table 1). We first examine the correlations among riverine input and nutrient, phytoplankton, and zooplankton concentrations on the LATEX shelf. We note that our simulation spans 2004–2010. It partially overlaps with the modeling period (1990–2004) of Fennel et al. (2011), allowing some comparisons to be drawn between the two studies.

Concentrations of DIN, phytoplankton and zooplankton (surface values, unless otherwise stated) were spatially averaged for each of the 3 sub-regions on the LATEX shelf.

BGD
10, 7785–7830, 2013

The resulting time series were then temporally averaged to come up with monthly mean values. Clear seasonality could be seen in monthly mean riverine nutrient input as well as in the monthly averaged nutrient ($NO_3 + NH_4$), phytoplankton, and zooplankton concentration on the LATEX shelf (Fig. 9). The maximum riverine nutrient input occurred in May, preceding the nutrient, phytoplankton and zooplankton peaks by one month to two months. Nutrient, phytoplankton and zooplankton concentrations were characterized by a clear decreasing trend from Delta to Intermediate, and further to the Far-field region. The correlation coefficient between the riverine nitrogen loading and nutrient concentration time series was 0.85 for the Delta, 0.67 for the Intermediate, and 0.27 for the Far-field region. The significant reduction in correlation in the Far-field region was consistent with the findings of Lehrter et al. (2009), who reported that there was no clear relationship between Mississippi river nutrient loading and regional-wide primary production on the LATEX shelf.

The influence of river plumes is typically limited within the inner/mid shelf (< 50 m water depth) in the GoM (e.g. Morey et al., 2003). Both satellite-derived and model-simulated surface chlorophyll maps (Fig. 8) were consistent with the presence of high chlorophyll concentration mainly located near the coast. In the following section, we separate the Gulf into shelf and deep-ocean regions using the 50 m isobath as the demarcation line. We consider the temporal variations of nutrient and plankton concentrations in each region and their dominant modes of variability.

Consistent with what we found on the LATEX shelf, nutrient, phytoplankton and zooplankton concentrations in the GoM shelves are strongly correlated with coastal river input (Fig. 10a, correlation coefficient: 0.91). The maximum riverine freshwater and nutrient input was seen in July 2008 (largely contributed by the 2008 Mississippi River flooding), along with high nutrient, phytoplankton and zooplankton concentrations on the shelf. Surface nutrient concentrations in the deep-ocean were limited (to ~ 1/10 of the inner shelf) and show no clear correlation with riverine input. The only exception to this was in summer 2008 when nutrient values peaked in association with the flooding of Mississippi River, which increased nutrient loading and contributed to higher nutrient

BGD
10, 7785–7830, 2013

concentrations offshore. Unlike on the shelf, nutrient concentrations in the deep ocean were seen to increase around January when wind mixing was stronger (Jolliff et al., 2008). A high nutrient peak appeared around February 2010, which was also observed during a March 2010 cruise and was related to wind-driven transport of the plume to normally oligotrophic offshore waters (Huang et al., under revision). Because of the enhanced biological activity as a result of plume nutrient transport, an unusually high CO_2 sink was also observed during that cruise. Surface phytoplankton concentrations in the deep-ocean were $\sim 0.5\,\mathrm{mmol\,N\,m^{-3}}$, about 50 % of that on the shelf (Fig. 10b), and lagged the temporal variations in nutrients by ∼ one month (Fig. 10c). Zooplankton concentrations in the deep-ocean were $\sim 0.01\,\mathrm{mmol\,N\,m^{-3}}$, about 20 % of that on the shelf (Fig. 10d).

To quantify the intrinsic linkages between nutrient and plankton variability, we removed their temporal mean (2005–2010) and applied an Empirical Orthogonal Function (EOF) analysis to their residuals. The temporal mean nutrient and phytoplankton fields resembled each other, both showing high values on the shelf (Fig. 11, upper panels). The mean zooplankton had elevated concentration in the northern GoM. The first EOF mode of the nutrient (phytoplankton, zooplankton) accounted for 76 % (50 %, 80 %) of their respective variance. Their corresponding first principal components (PC1) displayed clear seasonal cycles. Nutrient, phytoplankton, and zooplankton concentrations each reached their peak values in May-June, June, June-July, respectively. Together, surface nutrient, phytoplankton and zooplankton concentrations showed a phase-locked pattern. The nutrient variations generally lead phytoplankton variations by 0–1 month, which in turn lead zooplankton variations by 0–1 month. The second EOF modes of nutrient, phytoplankton, and zooplankton accounted for 19 %, 34 %, and 14 % of their respective variances, representing other higher order dynamical processes.

BGD
10, 7785–7830, 2013

4.2 Shelf nutrient budget

Monthly means (averaged over 2005–2010) of simulated cross-shelf velocity and nutrient flux at the 50 m isobath in the Gulf exhibited distinct temporal patterns (Fig. 12). Although the depth integrated current shows significant variability along the 50 m isobath, both DIN and particular organic nitrogen (PON hereafter) fluxes were dominated by an overall offshore transport (from shelf to deep-ocean, Fig. 12b, c, and d). Compared with DIN, the monthly climatology of the PON flux was more similar to the cross-shelf current climatology. This may be explained by the observation that transport of PON was predominantly associated with surface waters, making PON transport more sensitive to surface wind and current forcing; in contrast, the higher DIN concentrations in deep water resulted in DIN transport being more strongly influenced by deep water movements. A similar nutrient transport pattern has also been reported in the Middle Atlantic Bight (Fennel et al., 2006). Along the 50 m isobath, substantial cross-shelf nutrient exchange was found to the southeast of the Mississippi River mouth. Overall the shelf waters receive 135.87×10^9 mol nitrogen per year from rivers (estimated by river nitrogen concentration × freshwater discharge × time), and export 24.93×10^9 mol nitrogen (10.49×10^9 mol DIN and 14.44×10^9 mol PON) to the deep ocean (see: Tables 1 and 2).

The factors that determine water transport and nutrient fluxes in the Gulf can be explored by examining the shelf circulation and wind forcing on a region-by-region basis. To do that we generated seasonal means of surface wind and surface currents by averaging our 6 yr (2005–2010) model hindcast solutions. We found that the surface wind shows a similar spatial and temporal pattern with the COADS wind climatology (DaSilva et al., 1994). Shelf circulation is mainly wind-driven and the circulation pattern is generally consistent with a previous GoM modeling study covering the period of 1994–2004 by Morey et al. (2005).

Using the 50 m isobath as the boundary between the inner shelf and deep ocean, we can divide the shelf areas in the Gulf into 4 major sections (see Fig. 2): (1) the

BGD
10, 7785–7830, 2013

Bay of Campeche shelf (BOC) hereafter, (bounded by the 50 m isobath between 0 and 1000 km starting from the Campeche Bank, Fig. 13), (2) the Tamaulipas-Veracruz shelf (TAVE shelf hereafter, bounded by the 50-m isobath between 1000 and 1850 km, Fig. 14), (3) the LATEX shelf (bounded by the 50 m isobath between 1850 and 3000 km, Fig. 15), and (4) the West Florida Shelf (WFS hereafter, bounded by the 50 m isobath between 3000 and 4000 km, Fig. 16). Within each section, the nutrient flux between the shelf waters and deep-ocean (cross-shelf) as well as between different sections (along-shelf) can be assessed in conjunction with local riverine nutrient input, denitrification, and dominant physical transport processes (Tables 1 and 2).

4.2.1 BOC shelf

BOC is the southernmost semi-enclosed region in the GoM. Estimated nitrogen loading was 12.42×10^9 mol N yr^{-1} (Tables 1 and 2), the majority of which was discharged by the Usumacinta River. Mean (averaged over 2005-2010) nitrogen loading in spring, summer, fall, and winter were 1.41, 4.30, 4.19 and 2.52×10^9 mol N respectively. Consistent with findings of earlier studies (Zavala-Hidalgo et al., 2003; Morey et al., 2005), our results identify two prevailing circulation patterns in the BOC. In the northeast, upwelling favorable winds and upcoast currents (flowing in the direction with coast to the left) occupy the Campeche Bank throughout the year. The westward winds and associated current induced significant along-shelf transport, bringing 8.40×10^9 mol N yr^{-1} (DIN and PON combined, unless otherwise indicated) into the BOC at the east end of the BOC shelf (Fig. 13). West of the Campeche Bank the coastline is directed north-south, thus the westward current induced an overall offshore nutrient flux throughout the year (7.82×10^9 mol N yr^{-1}). In the center of the BOC, there is a permanent wind-driven cyclonic circulation (Vazquez de la Cerda et al., 2005), which tends to enhance during autumn to winter months. At the same time, a strong downcoast (flowing in the direction with coast to the right) current traveled into the southernmost part of the BOC (Fig. 13c), causing a local convergence on the inner shelf. This along-shelf current transported 0.17×10^9 mol N from the TAVE shelf to the BOC shelf. In the following

BGD
10, 7785–7830, 2013

winter, spring, and summer months, offshore cyclonic circulation weakened, while the upcoast current from the Campeche Bank gradually strengthened (Figs. 13a, b and d), transporting 0.17×10^9 mol nitrogen back to the TAVE shelf (winter, spring, and summer months combined). The BOC had the smallest denitrification rate among the four shelf sections (0.48 mmol N m^{-2} d^{-1}, multi-year mean, Table 2). The rate peaks during summer months (0.78 mmol N m^{-2} d^{-1}). The total amount of the DIN removed by denitrification was 12.85×10^9 mol N yr^{-1}, which closely balanced the nitrogen loading from local rivers.

4.2.2 TAVE shelf

The TAVE shelf has no major river, and thus received the least riverine nitrogen input into the GoM (~ only 1.83×10^9 mol N yr^{-1}, Table 2). Our results confirm that the circulation in the TAVE shelf (Fig. 14) is characterized by a flow reversal from upcoast circulation in spring-summer season to downcoast circulation in fall-winter season (Zavala-Hidalgo et al., 2003; DiMarco et al., 2005; Vazquez de la Cerda et al., 2005; Morey et al., 2005). During spring the shelf was characterized by easterly winds, upcoast currents, and an offshore nutrient transport of 0.12×10^9 mol N. The upcoast currents peaked during summer months when southeasterly wind prevails, transporting 1.5×10^9 mol nitrogen to the LATEX shelf. This strong southeasterly wind also induced strong shoreward nutrient flux (4.07×10^9 mol N in summer). In fall, easterly to northeast wind prevailed both the TAVE shelf and the LATEX shelf to the north, reversing the coastal flow on the TAVE shelf from the upcoast direction to the downcoast direction. Along-shelf currents from the LATEX shelf brought 4.55×10^9 mol nitrogen (fall and winter combined) to the TAVE shelf. The downcoast flow is accompanied by a net offshore nutrient flux in fall and winter, which amounted to 3.69×10^9 mol N to the deep sea. Due to the limited width, the amount of the DIN denitrified in the TAVE shelf was smallest among the four shelf sections (6.25×10^9 mol N yr^{-1}, Table 2).

BGD
10, 7785–7830, 2013

4.2.3 LATEX shelf

Our calculations indicated that the LATEX shelf received 0.78 billion tons of freshwater and 108.86×10^9 mol N annually (averaged over 2005–2010). More than 90 % of these river inputs were from the Mississippi/Atchafalaya river system, which had peak discharge values in spring months (42.68×10^9 mol N, Tables 1 and 2). Despite the large riverine input, ~67.7 % of the nitrogen was denitrified on the inner shelf (73.66×10^9 mol N yr^{-1}, Table 2). Of the remaining fraction, ~21.7 % (23.73×10^9 mol N yr^{-1}) was transported to either the TAVE shelf in the west or the WFS in the east through along-shelf flows; ~12.0 % (13.1×10^9 mol N yr^{-1}) was exported offshore to the deep ocean, mainly in association with waters southwest of the Mississippi River delta (Figs. 8 and 15).

Our results confirm that the inner LATEX shelf is dominated by downcoast winds in non-summer months (e.g. Cho et al., 1998; Zavala-Hidalgo et al., 2003; Morey et al., 2005; Figs. 15a, c and d). The correlation between monthly averaged currents and along-shelf wind stress was positive and highly significant (Nowlin et al., 2005). In spring, the upcoast currents from the northern TAVE shelf encountered the downcoast currents from the LATEX shelf, forming a confluence zone, where a high chlorophyll anomaly can be identified in the monthly climatology of SeaWiFS ocean color maps (Martinez-Lopez and Zavala-Hidalgo, 2009). However, no prominent offshore transport was seen in either seasonal chlorophyll climatology (Fig. 8) or cross-shelf velocity (Fig. 12a) at this location.

The outer LATEX shelf is more influenced by its interaction with Loop Current Eddies (e.g., Ohlmann et al., 2001; Nowlin et al., 2005), which can bring large temporal and spatial variability to the current fields along the 50 m isobath. Despite such variability, strong offshore nutrient export was seen in areas around the Mississippi Delta almost throughout the year (Fig. 12). In addition to offshore nutrient export, the LATEX shelf continuously delivered nutrient to the adjacent TAVE shelf (5.19×10^9 mol N, fall, winter, and spring combined) and WFS (20.22×10^9 mol N yr^{-1}) almost throughout

BGD
10, 7785–7830, 2013

the year. As previously described, westward along-shelf flow on the western LATEX shelf during non-summer months continuously transported nutrients to the TAVE shelf. The only exception was during summer months when the winds changed to northwestward, and currents on the western LATEX shelf shifted to the upcoast direction (Fig. 15b). East of the Mississippi delta, the along-shelf currents also flowed eastward, transporting nutrient from LATEX shelf to WFS. This nutrient flux reached its annual maximum (8.81×10^9 mol N) in summer.

4.2.4 WFS

Circulation of the WFS was influenced by both local and deep–ocean LC forcing. Our 6 yr mean wind and surface current fields (Fig.16) reproduced many known features identified in earlier studies (e.g. He and Weisberg, 2002, 2003; Weisberg et al., 2005). Annual riverine nitrogen input (12.76×10^9 mol N yr^{-1}) on the WFS was comparable to those on the BOC shelf (12.42×10^9 mol N yr^{-1}, Table 2). The riverine nitrogen loading peaks in summer months (7.27×10^9 mol N). Depth integrated currents and nutrient flux at the 50 m isobath were characterized by significant spatial variability at the Mississippi-Alabama-Florida junction and a mean offshore transport on the west Florida (Fig. 12). Previous studies provided evidence that the shelf off the Mississippi-Alabama-Florida junction receives a large amount of low salinity water from the Mississippi River during summer months (e.g., Morey et al., 2003, 2005). A low salinity "tongue" is formed as a result of intensive cross-shelf freshwater export (e.g., Morey et al., 2003) and can be identified as a patch of high chlorophyll waters flowing to the south/southeast (Fig. 8). The 6 yr mean offshore nutrient flux was 4.24×10^9 mol N yr^{-1}. Unlike the LATEX shelf, the offshore nutrient flux at WFS is dominated by PON export (~96.7 %). Not surprisingly, the along-shelf nutrient flux from the LATEX shelf (20.22×10^9 mol N yr^{-1}) is the major nutrient source for the WFS. Together with local river inputs, the majority of the nutrients transported from the LATEX shelf to the broad WFS was denitrified (24.27×10^9 mol N yr^{-1}, Table 2).

BGD
10, 7785–7830, 2013

In summary, our calculations show that the GoM shelf receives 142.88×10^9 mol N nutrient annually, the majority of which was input by local rivers (135.87×10^9 mol N yr^{-1}). On an annual basis, over 80 % of these nutrients were denitrified on the shelf (117.04×10^9 mol N yr^{-1}). The shelf-wide denitrification rate was estimated to be 1.04 mmol N m^{-2} d^{-1}, which was comparable to that in the Middle Atlantic Bight (0.92 mmol N m^{-2} d^{-1}, Fennel et al., 2008). Among the four shelf sections, the LATEX shelf has the highest denitrification rate (1.84 mmol N m^{-2} d^{-1}) corresponding to the largest local river inputs. For both WFS and TAVE shelves, a large part of the denitrified nitrogen was from the adjacent LATEX shelf through along-shelf transport. On the BOC shelf, besides local river inputs, an important nutrient source was the PON transported in the along-shelf direction from the Campeche Bank.

Our calculations also support the view that the Gulf-wide mean cross-shelf nutrient exchange between the inner shelf and deep-ocean is seaward. On an annual basis, the amount of the nitrogen exported from the shelf (24.93×10^9 mol N yr^{-1}) was about ~ 17 % of that received from local rivers and along-shelf transport. Across-shelf nitrogen flux changes its onshore/offshore direction seasonally on the TAVE shelf and WFS, but remains persistently offshore on LATEX and BOC shelves.

5 Summary and conclusions

We have coupled a 7-component marine ecosystem model with a three-dimensional high-resolution circulation model for the Gulf of Mexico and South Atlantic Bight. The coupled physical-biogeochemical modeling system was used to hindcast the GoM circulation and biogeochemical variations from January 2004 to December 2010. Favorable comparisons were found when validating model hindcast solutions against satellite observed surface chlorophyll and sea-level, and extensive in-situ measurements including sea-level, temperature, salinity, and nutrients, indicating that the coupled model can resolve the major physical and biogeochemical dynamics in the GoM. Time and space continuous hindcast fields from January 2005 to December 2010 were then

BGD
10, 7785–7830, 2013

used to investigate the temporal and spatial characteristics of the GoM circulation and ecosystem variability.

Clear seasonality and interannual variability was seen in riverine freshwater and nutrient input. While significant temporal correlations were found between riverine nutrient input and nutrient concentration on the shelf, no clear correlation was seen between river nutrient loading and surface nutrient concentration in the deep ocean. EOF analyses revealed that the largest variability in nutrient and plankton distributions occurred in the northern GoM. PC1s of the EOF analyses were indicative of a phase-locked pattern among nutrient, phytoplankton and zooplankton concentrations: the nutrient variations generally lead phytoplankton variations by 0–1 month, which in turn lead zooplankton variations by 0–1 month.

A shelf nitrogen budget was developed based on the multi-year mean conditions over 2005–2010. Based on our estimated flux, we concluded that the majority of the riverine nitrogen load is denitrified on the inner shelf. Along-shelf transport played an important role in distributing the large nitrogen load in the LATEX shelf to adjacent WFS and TAVE shelves. Persistent cross-shelf exchange was seen between the shelf and deep-ocean. Regions off the BOC, Mississippi River Delta and in Mississippi-Alabama-Florida junction were identified as major nutrient export sites. On an annual basis, the amount of exported nutrients was equivalent to 17 % of that received from rivers and along-shelf transport.

Our study provides a modeling framework to examine important hydrologic-physical-biogeochemical coupling processes in the GoM, allowing for an integrated understanding of regional marine ecosystem responses to a broad spectrum of processes, ranging from extreme synoptic weather events (e.g., hurricanes) to climate and land use changes. We note however that the complexity of the food web and uncertainties in model parameterizations remain an active research topic in coupled physical-biogeochemical modeling. For instance, we have not considered the process of nitrogen fixation process by cyanobacteria (Walsh et al., 1989; Mulholland et al., 2006) in this study. The lack of accounting for phosphate and silicate compartments in the

BGD
10, 7785–7830, 2013

ecosystem model may compromise the model ability and accuracy in simulating plankton population dynamics. Improved marine biogeochemical modeling skill can be further achieved with refinement of model process/parameterizations and advances in observational infrastructure (e.g. more rapid and accurate nutrient sensors) together with sophisticated techniques for data assimilation.

Acknowledgements. Research support provided through NASA Grants 09-IDS09-0040, 11-CMS11-003, and NNX10AU06G; NOAA Grant IOOS-2011-2002515; and GRI GISR grant 12-09/GoMRI-006 is much appreciated.

References

Aulenbach, B. T., Buxton, H. T., Battaglin, W. T., and Couple, R. H: Streamflow and nutrient fluxes of the Mississippi-Atchafalaya River Basin and subbasins for the period of record through 2005: US Geological Survey Open-File Report 2007-1080 2007.

Bianchi, T., DiMarco, S., Cowan Jr., J., Hetland, R., Chapman, P., Day, J., and Allison, M.: The science of hypoxia in the Northern Gulf of Mexico: a review, Sci. Total Environ., 408, 2010.

Cai, W.-J., Hu, X., Huang, W.-J., Murrell, M. C., Lehrter, J. C., Lohrenz, S. E., Chou, W.-C., Zhai, W., Hollibaugh, J. T., Wang, Y., Zhao, P., Guo, X., Gundersen, K., Dai, M., and Gong, G.-C.: Acidification of subsurface coastal waters enhanced by eutrophication, Nat. Geosci., 4, 766–770, 2011.

CENR (Committee on Environmental and Natural Resources): Integrated Assessment of Hypoxia in the Northern Gulf of Maxico, Washington, DC, 48, 2000.

Chassignet, E. P., Hurlburt, H. E., Smedstad, O. M., Halliwell, G. R., Hogan, P. J., Wallcraft, A. J., Baraille, R., and Bleck, R.: The HYCOM (HYbrid Coordinate Ocean Model) data assimilative system, J. Mar. Syst., 65, 60–83, 2007.

Cho, K. W., Reid, R. O., and Nowlin, W. D.: Objectively mapped stream function fields on the Texas-Louisiana shelf based on 32 months of moored current meter data, J. Geophys. Res.-Oceans, 103, 10377–10390, 1998.

DaSilva, A., Younga, A. C., and Levitus, S.: Atlas of Surface Marine Data 1994, Volume 1: Algorithms and Procedures, 1994.

BGD
10, 7785–7830, 2013

DiMarco, S., Nowlin, W., and Reid, R. O.: A statistical description of the velocity fields from upper ocean drifter in the Gulf of Mexico, in: Circulation in the Gulf of Mexico: Observations and Models, Geophys. Monogr. Ser., AGU, Washington, DC, 101–110, 2005.

DiMarco, S. F., Chapman, P., Walker, N., and Hetland, R. D.: Does local topography control hypoxia on the eastern Texas-Louisiana shelf?, J. Mar. Syst., 80, 25–35, 2010.

Egbert, G. D. and Erofeeva, S. Y.: Efficient Inverse Modeling of Barotropic Ocean Tides, J. Atmos. Ocean. Technol., 19, 183–204, doi:10.1175/1520-0426(2002)019<0183:EIMOBO>2.0.CO;2, 2002.

Fennel, K., Wilkin, J., Levin, J., Moisan, J., O'Reilly, J., and Haidvogel, D. B.: Nitrogen cycling in the Middle Atlantic Bight: results from a three-dimensional model and implications for the North Atlantic nitrogen budget, Global Biogeochem. Cy., 20, GB3007, doi:10.1029/2005GB002456, 2006.

Fennel, K., Wilkin, J., Previdi, M., and Najjar, R.: Denitrification effects on air-sea CO_2 flux in the coastal ocean: simulations for the Northwest North Atlantic, Geophys. Res. Lett., 35, L24608, doi:10.1029/2008GL036147, 2008.

Fennel, K., Hetland, R., Feng, Y., and DiMarco, S.: A coupled physical-biological model of the Northern Gulf of Mexico shelf: model description, validation and analysis of phytoplankton variability, Biogeosciences, 8, 1881–1899, doi:10.5194/bg-8-1881-2011, 2011.

Fennel, K., Hu, J., Laurent, A., Marta-Almeida, M., and Hetland, R.: Sensitivity of hypoxia predictions for the northern Gulf of Mexico to sediment oxygen consumption and model nesting, J. Geophys. Res.-Oceans, 118, 990–1002, doi:10.1002/jgrc.20077, 2013.

Flather, R. A.: A tidal model of the northwest European continental shelf, Memoires de la Societe Royale de Sciences de Liege, 141–164, 1976.

Fuentes-Yaco, C., de Leon, D. A. S., Monreal-Gomez, M. A., and Vera-Herrera, F.: Environmental forcing in a tropical estuarine ecosystem: the Palizada River in the southern Gulf of Mexico, Mar. Freshwater Res., 52, 735–744, 2001.

Garcia, H. E., Locarnini, R. A., Boyer, T. P., Antonov, J. I., Zweng, M. M., Baranova, O. K., and Johnson, D. R.: World Ocean Atlas 2009, NOAA Atlas NESDIS 71, edited by: Levitus, S., US Government Printing Office, Washington, DC, 398 pp., 2010.

Gattuso, J. P., Frankignoulle, M., and Wollast, R.: Carbon and Carbonate Metabolism in Coastal Aquatic Ecosystems, Annu. Rev. Ecol. Syst., 29, 405–434, 1998.

Gilbes, F., Tomas, C., Walsh, J. J., and Muller-Karger, F. E.: An episodic chlorophyll plume on the West Florida Shelf, Cont. Shelf Res., 16, 1201–1224, 1996.

BGD
10, 7785–7830, 2013

Goolsby, D. A., Battaglin, W. A., Aulenbach, B. T., and Hooper, R. P.: Nitrogen input to the Gulf of Mexico, J. Environ. Qual., 30, 329–336, 2001.

Guo, X. H., Cai, W. J., Huang, W. J., Wang, Y. C., Chen, F. Z., Murrell, M. C., Lohrenz, S. E., Jiang, L. Q., Dai, M. H., Hartmann, J., Lin, Q., and Culp, R.: Carbon dynamics and community production in the Mississippi River plume, Limnol. Oceanogr., 57, 1–17, 2012.

Haidvogel, D. B., Arango, H., Budgell, W. P., Cornuelle, B. D., Curchitser, E., Di Lorenzo, E., Fennel, K., Geyer, W. R., Hermann, A. J., Lanerolle, L., Levin, J., McWilliams, J. C., Miller, A. J., Moore, A. M., Powell, T. M., Shchepetkin, A. F., Sherwood, C. R., Signell, R. P., Warner, J. C., and Wilkin, J.: Ocean forecasting in terrain-following coordinates: Formulation and skill assessment of the Regional Ocean Modeling System, J. Comput. Phys., 227, 3595–3624, 2008.

He, R. Y. and Weisberg, R. H.: West Florida shelf circulation and temperature budget for the 1999 spring transition, Cont. Shelf Res., 22, 719–748, 2002.

He, R. Y. and Weisberg, R. H.: West Florida shelf circulation and temperature budget for the 1998 fall transition, Cont. Shelf Res., 23, 777–800, 2003.

Heileman, S. and Rabalais, N.: XV-50 Gulf of Mexico LME, United Nations Environment Programme, Nairobi, Kenya, 673–688, 2008.

Huang, W.-J., Cai, W.-J., Powell, R. T., Lohrenz, S. E., Wang, Y., Jiang, L.-Q., and Hopkinson, C. S.: The stoichiometry of inorganic carbon and nutrient removal in the Mississippi River plume and adjacent continental shelf, Biogeosciences, 9, 2781–2792, doi:10.5194/bg-9-2781-2012, 2012.

Huang, W. J., Cai, W. J., Casttelao, R. M., Wang, Y., and Lohrenz, S. E.: Impacts of a wind-driven cross-shelf large river plume on biological production and CO_2 update in the Gulf of Mexico during spring, Limnol. Oceanogr., in review, 2013.

Hyun, K. H. and He, R.: Coastal upwelling in the South Atlantic Bight: A revisit of the 2003 cold event using long term observations and model hindcast solutions, J. Mar. Syst., 83, 1–13, 2010.

Jolliff, J. K., Walsh, J. J., He, R. Y., Weisberg, R., Stovall-Leonard, A., Coble, P. G., Conmy, R., Heil, C., Nababan, B., Zhang, H. Y., Hu, C. M., and Muller-Karger, F. E.: Dispersal of the Suwannee River plume over the West Florida shelf: Simulation and observation of the optical and biochemical consequences of a flushing event, Geophys. Res. Lett., 30, 1709, doi:10.1029/2003GL016964, 2003.

BGD
10, 7785–7830, 2013

Jolliff, J. K., Kindle, J. C., Penta, B., Helber, R., Lee, Z., Shulman, I., Arnone, R., and Rowley, C. D.: On the relationship between satellite-estimated bio-optical and thermal properties in the Gulf of Mexico, J. Geophys. Res.-Biogeo., 113, G01024, doi:10.1029/2006JG000373, 2008.
Laurent, A., Fennel, K., Hu, J., and Hetland, R.: Simulating the effects of phosphorus limitation in the Mississippi and Atchafalaya River plumes, Biogeosciences, 9, 4707–4723, doi:10.5194/bg-9-4707-2012, 2012.
Lehrter, J. C., Murrell, M. C., and Kurtz, J.: Interactions between freshwater input, light, and phytoplankton dynamics on the Louisiana continental shelf, Cont. Shelf Res., 29, 1861–1872, 2009.
Lehrter, J. C., Beddick, D. L., Devereux, R., Yates, D. F., and Murrell, M. C.: Sediment-water fluxes of dissolved inorganic carbon, O-2, nutrients, and N-2 from the hypoxic region of the Louisiana continental shelf, Biogeochemistry, 109, 233–252, 2012.
Liu, K. K., Atkinson, L. P., Quinones, R., and Talaue-McManus, L.: Carbon and Nutrient Fluxes in Continental Margins: A Global Synthesis, IGBP Book Series, Springer, Berlin, 2010.
Lohrenz, S. E., Fahnenstiel, G. L., Redalje, D. G., Lang, G. A., Chen, X. G., and Dagg, M. J.: Variations in primary production of northern Gulf of Mexico continental shelf waters linked to nutrient inputs from the Mississippi River, Mar. Ecol.-Prog. Ser., 155, 45–54, 1997.
Lohrenz, S., Fahnenstiel, G., Redalje, D., Lang, G., Dagg, M., Whitledge, T., and Dortch, Q.: Nutrients, irradiance, and mixing as factors regulating primary production in coastal waters impacted by the Mississippi River plume, Cont. Shelf Res., 19, 1113–1141, 1999.
Lohrenz, S. E., Redalje, D. G., Cai, W. J., Acker, J., and Dagg, M.: A retrospective analysis of nutrients and phytoplankton productivity in the Mississippi River plume, Cont. Shelf Res., 28, 1466–1475, 2008.
Marchesiello, P., McWilliams, J. C., and Shchepetkin, A.: Open boundary conditions for long-term integration of regional oceanic models, Ocean Model., 3, 1–20, 2001.
Martinez-Lopez, B. and Zavala-Hidalgo, J.: Seasonal and interannual variability of cross-shelf transports of chlorophyll in the Gulf of Mexico, J. Mar. Syst., 77, 1–20, 2009.
Mellor, G. L. and Yamada, T.: Development of a turbulence closure model for geophysical fluid problems, Rev. Geophys., 20, 851–875, 1982.
Milliman, J. D. and Farnsworth, K. L.: River discharge to the coastal ocean: a global synthesis, Cambridge University Press, Cambridge, New York, viii, 384 pp., 2011.

BGD
10, 7785–7830, 2013

Morey, S. L., Martin, P. J., O'Brien, J. J., Wallcraft, A. A., and Zavala-Hidalgo, J.: Export pathways for river discharged fresh water in the northern Gulf of Mexico, J. Geophys. Res.-Oceans, 108, 3303, doi:10.1029/2002JC001674, 2003.

Morey, S. L., Zavala-Hidalgo, J., and O'Brien, J. J.: The seasonal variability of continental shelf circulation in the northern and western Gulf of Mexico from a high-resolution numerical model, in: Circulation in the Gulf of Mexico: Observations and Models, Geophys. Monogr. Ser., AGU, Washington, DC, 203–218, 2005.

Mulholland, M. R., Bernhardt, P. W., Heil, C. A., Bronk, D. A., and O'Neil, J. M.: Nitrogen fixation and release of fixed nitrogen by Trichodesmium spp. in the Gulf of Mexico, Limnol. Oceanogr., 51, 1762–1776, 2006.

Muller-Karger, F. E., Walsh, J. J., Evans, R. H., and Meyers, M. B.: On the Seasonal Phytoplankton Concentration and Sea-Surface Temperature Cycles of the Gulf of Mexico as Determined by Satellites, J. Geophys. Res.-Oceans, 96, 12645–12665, 1991.

Nababan, B., Muller-Karger, F. E., Hu, C., and Biggs, D. C.: Chlorophyll variability in the northeastern Gulf of Mexico, Int. J. Remote Sens., 32, 8373–8391, doi:10.1080/01431161.2010.542192, 2011.

Nixon, S. W., Ammerman, J. W., Atkinson, L. P., Berounsky, V. M., Billen, G., Boicourt, W. C., Boynton, W. R., Church, T. M., Ditoro, D. M., Elmgren, R., Garber, J. H., Giblin, A. E., Jahnke, R. A., Owens, N. J. P., Pilson, M. E. Q., and Seitzinger, S. P.: The fate of nitrogen and phosphorus at the land sea margin of the North Atlantic Ocean, Biogeochemistry, 35, 141–180, 1996.

Nowlin, W., Jochens, A. E., DiMarco, S., Reid, R. O., and Howard, M. K.: Low-frequency circulation over the Texas-Louisiana continental shelf, in: Circulation in the Gulf of Mexico: Observations and Models, Geophys. Monogr. Ser., AGU, Washington, DC, 219–240, 2005.

Ohlmann, J. C., Niiler, P. P., Fox, C. A., and Leben, R. R.: Eddy energy and shelf interactions in the Gulf of Mexico, J. Geophys. Res.-Oceans, 106, 2605–2620, 2001.

Rabalais, N., Turner, R. E., and Wiseman, W. J. J.: GULF OF MEXICO HYPOXIA, A.K.A. THE DEAD ZONE, Annu. Rev. Ecol. Syst., 33, 235–263, 2002.

Rabalais, N. N., Turner, R. E., Sen Gupta, B. K., Boesch, D. F., Chapman, P., and Murrell, M. C.: Hypoxia in the northern Gulf of Mexico: Does the science support the plan to reduce, mitigate, and control hypoxia?, Estuar. Coasts, 30, 753–772, 2007.

Seitzinger, S. P. and Giblin, A. E.: Estimating denitrification in North Atlantic continental shelf sediments, Biogeochemistry, 35, 235–260, 1996.

BGD
10, 7785–7830, 2013

Shchepetkin, A. F. and McWilliams, J. C.: The Regional Ocean Modeling System (ROMS): a split-explicit, free-surface, topography-following coordinates ocean model, Ocean Model., 9, 347–404, 2005.
Sturges, W. and Leben, R.: Frequency of Ring Separations from the Loop Current in the Gulf of Mexico: A Revised Estimate, J. Phys. Oceanogr., 30, 1814–1819, 2000.
Taylor, K. E.: Summarizing multiple aspects of model performance in a single diagram, J. Geophys. Res., 106, 7183–7192, 2001.
Toner, M., Kirwan, A. D., Poje, A. C., Kantha, L. H., Muller-Karger, F. E., and Jones, C. K. R. T.: Chlorophyll dispersal by eddy-eddy interactions in the Gulf of Mexico, J. Geophys. Res.-Oceans, 108, 3105, doi:10.1029/2002JC001499, 2003.
Turner, R. and Rabalais, N.: Suspended particulate and dissolved nutrient loadings to Gulf of Mexico estuaries, in: Biogeochemistry of Gulf of Mexico estuaries, edited by: Bianchi, T., Pennock, J., and Twilley, R., John Wiley & Sons, Inc., New York, 1999.
Vazquez de la Cerda, A. M., Reid, R. O., DiMarco, S. F., and Jochens, A. E.: Bay of Campeche circulation: An update, in: Circulation in the Gulf of Mexico: Observations and Models, Geophys. Monogr. Ser., AGU, Washington, DC, 279–293, 2005.
Walsh, J. J., Dieterle, D. A., Meyers, M. B., and Muller-karger, F. E.: Nitrogen exchange at the continental margin: A numerical study of the Gulf of Mexico, Progr. Oceanogr., 23, 245–301, 1989.
Weisberg, R., He, R. Y., Liu, Y. G., and Virmani, J. I.: West Florida Shelf circulation on synoptic, seasonal, and Interannual time scales, in: Circulation in the Gulf of Mexico: Observations and Models, Geophys. Monogr. Ser., AGU, Washington, DC, 325–347, 2005.
White, J. R., Fulweiler, R. W., Li, C. Y., Bargu, S., Walker, N. D., Twilley, R. R., and Green, S. E.: Mississippi River Flood of 2008: Observations of a Large Freshwater Diversion on Physical, Chemical, and Biological Characteristics of a Shallow Estuarine Lake, Environ. Sci. Technol., 43, 5599–5604, doi:10.1021/es900318t, 2009.
Wiseman, W. J., Rabalais, N. N., Turner, R. E., Dinnel, S. P., and MacNaughton, A.: Seasonal and interannual variability within the Louisiana coastal current: stratification and hypoxia, J. Mar. Syst., 12, 237–248, 1997.
Zavala-Hidalgo, J., Morey, S. L., and O'Brien, J. J.: Seasonal circulation on the western shelf of the Gulf of Mexico using a high-resolution numerical model, J. Geophys. Res., 108, 3389, doi:10.1029/2003JC001879, 2003.

BGD
10, 7785–7830, 2013

Table 1. River, cross-shelf (at 50 m isobath), along-shelf, and denitrification flux in the inner shelf.

	Nutrient Flux		Shelf*				
			BOC	TAVE	LATEX	WFS	Shelf-Wide
SPRING	River Input (mol N m^{-3} s^{-1})		0.91	0.33	5.32	0.79	7.34
	Cross-shelf** (mmol N m^{-1} s^{-1})	DIN	0.02	0.1	−0.26	0.06	−0.03
		PON	−0.21	−0.12	−0.12	−0.18	−0.16
	Along-shelf*** (mmol N m^{-1} s^{-1})	DIN	0.12	0.64	−2.56	2.16	0.07
		PON	3.11	1.07	−3.19	2.48	0.17
	Denitrification**** (mmol N m^{-2} d^{-1})		−0.53	−0.92	−2.49	−0.55	−1.28
SUMMER	River Input (mol N m^{-3} s^{-1})		1.13	0.37	5.21	0.99	7.69
	Cross-shelf (mmol N m^{-1} s^{-1})	DIN	−0.05	0.38	−0.48	−0.21	−0.12
		PON	−0.29	0.23	−0.19	−0.31	−0.15
	Along-shelf (mmol N m^{-1} s^{-1})	DIN	−0.27	0.25	−5.06	5.37	0.18
		PON	1.96	−0.93	−2.66	4.56	0.28
	Denitrification (mmol N m^{-2} d^{-1})		−0.74	−1.13	−2.39	−0.84	−1.4
FALL	River Input (mol N m^{-3} s^{-1})		0.58	0.21	3.75	0.5	5.04
	Cross-shelf (mmol N m^{-1} s^{-1})	DIN	−0.13	−0.07	−0.16	0.09	−0.07
		PON	−0.16	−0.1	0.04	0.01	−0.05
	Along-shelf (mmol N m^{-1} s^{-1})	DIN	1.0	0.49	−2.78	1.44	0.02
		PON	2.61	−0.59	−2.62	1.17	0.02
	Denitrification (mmol N m^{-2} d^{-1})		−0.37	−0.36	−1.12	−0.64	−0.73

BGD
10, 7785–7830, 2013

Table 1. Continued.

	Nutrient Flux		Shelf*				
			BOC	TAVE	LATEX	WFS	Shelf-Wide
WINTER	River Input (mol N m^{-3} s^{-1})		0.80	0.29	4.25	0.70	6.04
	Cross-shelf (mmol N m^{-1} s^{-1})	DIN	−0.02	−0.22	−0.24	0.03	−0.11
		PON	−0.16	−0.17	−0.05	−0.04	−0.1
	Along-shelf (mmol N m^{-1} s^{-1})	DIN	0.08	2.78	−5.61	2.89	0.05
		PON	0.86	1.77	−4.44	2.44	0.08
	Denitrification (mmol N m^{-2} d^{-1})		−0.28	−0.45	−1.36	−0.52	−0.76
ANNUAL	River Input (mol N m^{-3} s^{-1})		0.86	0.30	4.63	0.74	6.53
	Cross-shelf (mmol N m^{-1} s^{-1})	DIN	−0.04	0.05	−0.28	0	−0.08
		PON	−0.21	−0.04	−0.08	−0.13	−0.11
	Along-shelf (mmol N m^{-1} s^{-1})	DIN	0.23	1.04	−4.0	2.96	0.23
		PON	2.14	0.33	−3.23	2.67	1.90
	Denitrification (mmol N m^{-2} d^{-1})		−0.48	−0.72	−1.84	−0.64	−1.04

* Shelf abbreviations: BOC shelf: Bay of Campeche, TAVE: Tamaulipas-Veracruz shelf, LATEX: Louisiana-Texas shelf; WFS: West Florida Shelf.
** For cross-shelf DIN/PON transport, +: onshore, −: offshore.
*** For along-shelf DIN/PON transport, +: net gain, −: net lose.
**** Denitrification rates are presented in negative values as a nitrogen removal process.

BGD
10, 7785–7830, 2013

Table 2. River, cross-shelf (at 50 m isobath), along-shelf, and denitrification budget in the inner shelf.

	Nutrient Budget (10^9 mol N yr^{-1})		Shelf*				
			BOC	TAVE	LATEX	WFS	Shelf-Wide
SPRING	River Input		1.41	0.26	42.68	2.08	46.42
	Cross-shelf**	DIN	0.14	0.66	−2.32	0.5	−1.02
		PON	−1.68	−0.8	−1.05	−1.39	−4.93
	Along-shelf***	DIN	0.32	0.25	−2.15	1.87	0.29
		PON	3.06	0.44	−2.64	2.12	2.98
	Denitrification****		−3.56	−2.0	−24.93	−5.28	−35.77
SUMMER	River Input		4.30	0.59	26.31	7.27	38.47
	Cross-shelf	DIN	−0.37	2.52	−4.28	−1.63	−3.77
		PON	−2.24	1.55	−1.69	−2.46	−4.85
	Along-shelf	DIN	0.25	−0.19	−4.5	4.67	0.23
		PON	2.58	−1.2	−2.81	3.91	2.48
	Denitrification		−4.97	−2.46	−23.87	−7.97	−39.27
FALL	River Input		4.19	0.59	13.85	2.54	21.17
	Cross-shelf	DIN	−0.98	−0.45	−1.44	0.72	−2.15
		PON	−1.23	−0.64	0.36	0.07	−1.43
	Along-shelf	DIN	0.2	0.79	−2.12	1.25	0.12
		PON	0.65	0.78	−1.95	1.01	0.49
	Denitrification		−2.47	−0.79	−11.24	−6.08	20.59

BGD
10, 7785–7830, 2013

Table 2. Coninued.

	Nutrient Budget (10^9 mol N yr^{-1})		Shelf*				
			BOC	TAVE	LATEX	WFS	Shelf-Wide
WINTER	River Input		2.52	0.39	26.02	0.88	29.81
	Cross-shelf	DIN	−0.18	−1.45	−2.19	0.27	−3.55
		PON	−1.28	−1.15	−0.49	−0.31	−3.23
	Along-shelf	DIN	0.2	1.68	−4.28	2.45	0.05
		PON	0.74	1.14	−3.46	1.98	0.4
	Denitrification		−1.86	−0.99	−13.61	−4.94	−21.4
ANNUAL	River Input		12.42	1.83	108.86	12.76	135.87
	Cross-shelf	DIN	−1.4	1.28	−10.23	−0.14	−10.49
		PON	−6.43	−1.04	−2.87	−4.1	−14.44
	Along-shelf	DIN	0.97	2.52	−13.05	10.23	0.67
		PON	7.03	1.15	−10.68	9.02	6.34
	Denitrification		−12.85	−6.25	−73.66	−24.27	−117.04

* Shelf abbreviations: BOC: Bay of Campeche shelf, TAVE: Tamaulipas-Veracruz shelf, LATEX: Louisiana-Texas shelf; WFS: West Florida Shelf.
** For cross-shelf DIN/PON transport, +: onshore, −: offshore.
*** For along-shelf DIN/PON transport, +: net gain, −: net lose.
**** Denitrification budgets are presented in negative values as a nitrogen removal process.

BGD
10, 7785–7830, 2013

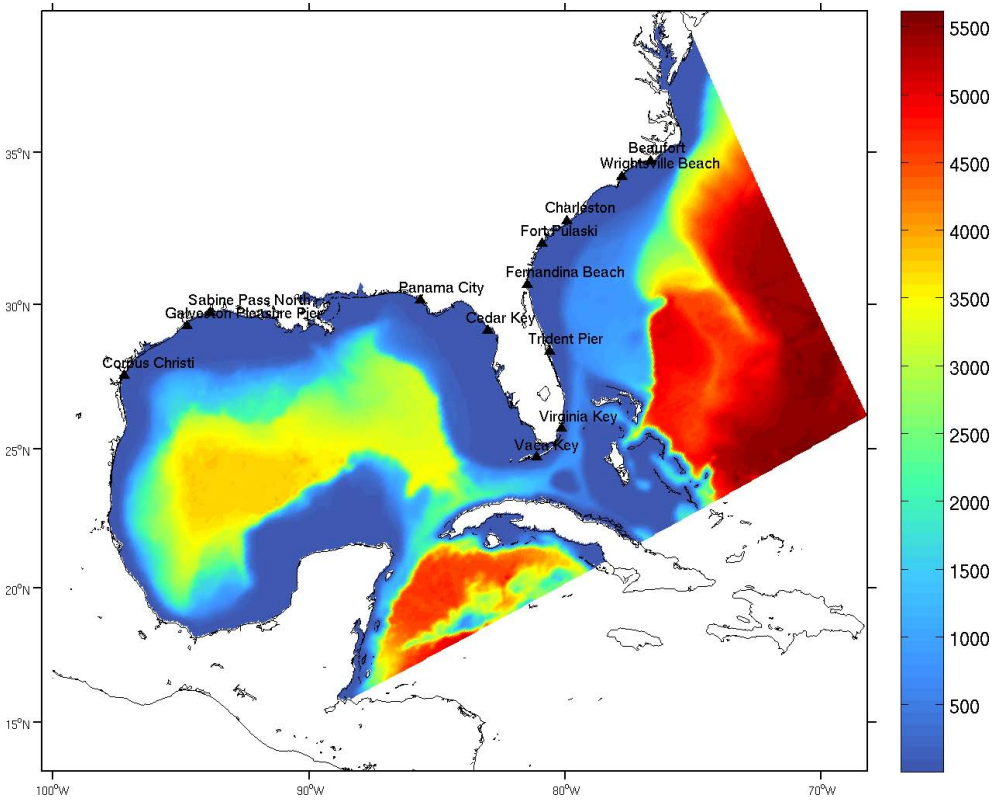

Fig. 1. The SABGOM ROMS model domain overlaid with water depth (color-shading) and location of 13 tidal stations (black triangles).

BGD
10, 7785–7830, 2013

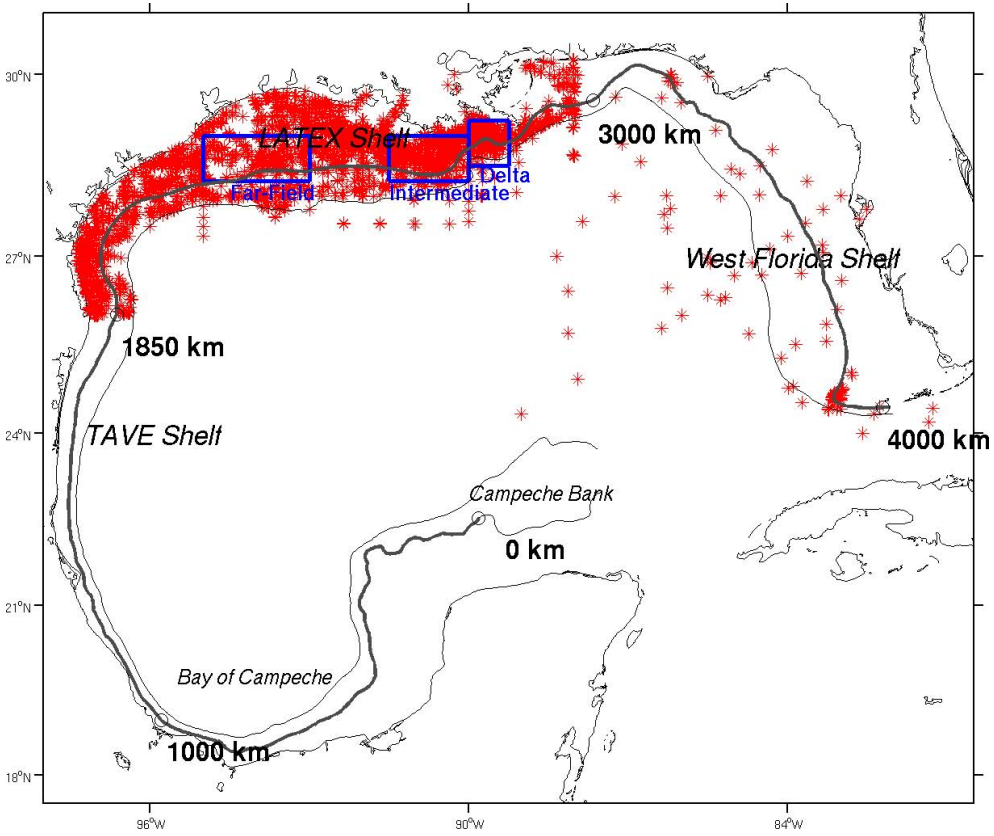

Fig. 2. Locations (star) of in-situ ship survey data. Also shown are the 50 m and 200 m isobath in the Gulf of Mexico, and the location of three sub-regions: Delta, Intermediate, and Far-field.

BGD
10, 7785–7830, 2013

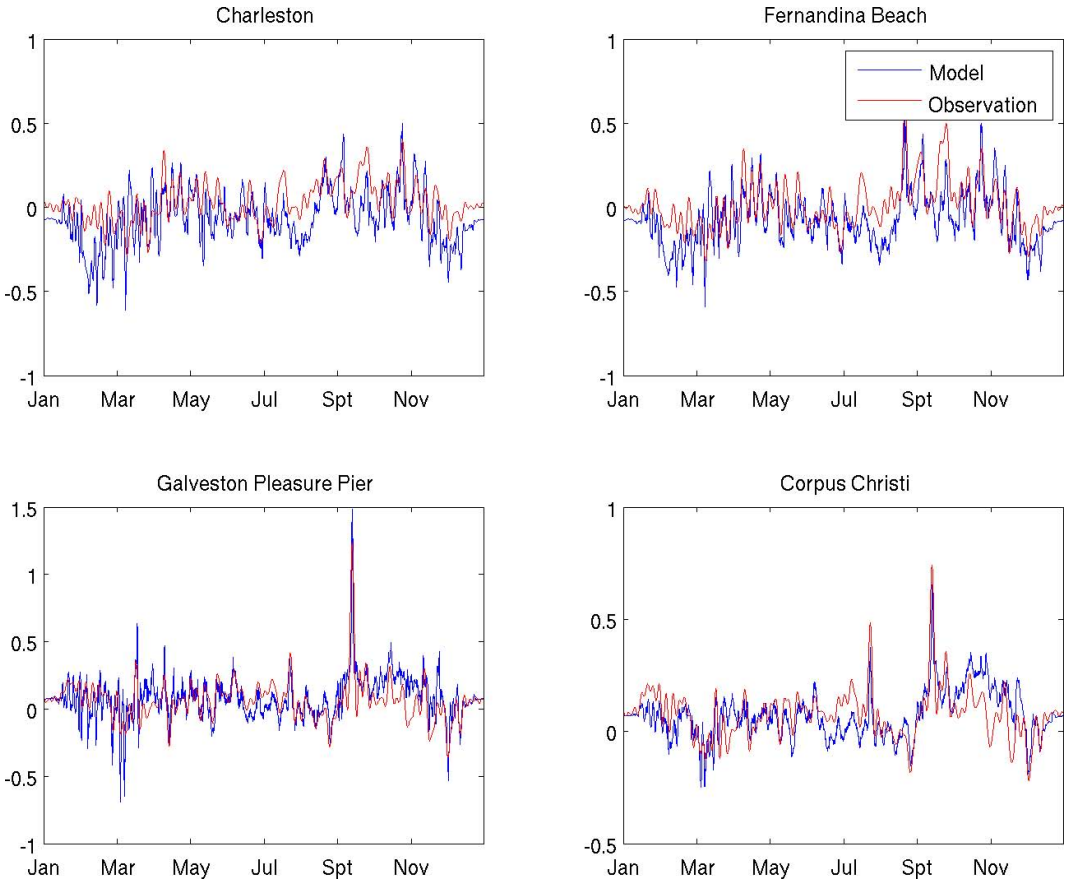

Fig. 3. Comparisons between observed and simulated sea-level time series at four tidal stations in 2008.

BGD
10, 7785–7830, 2013


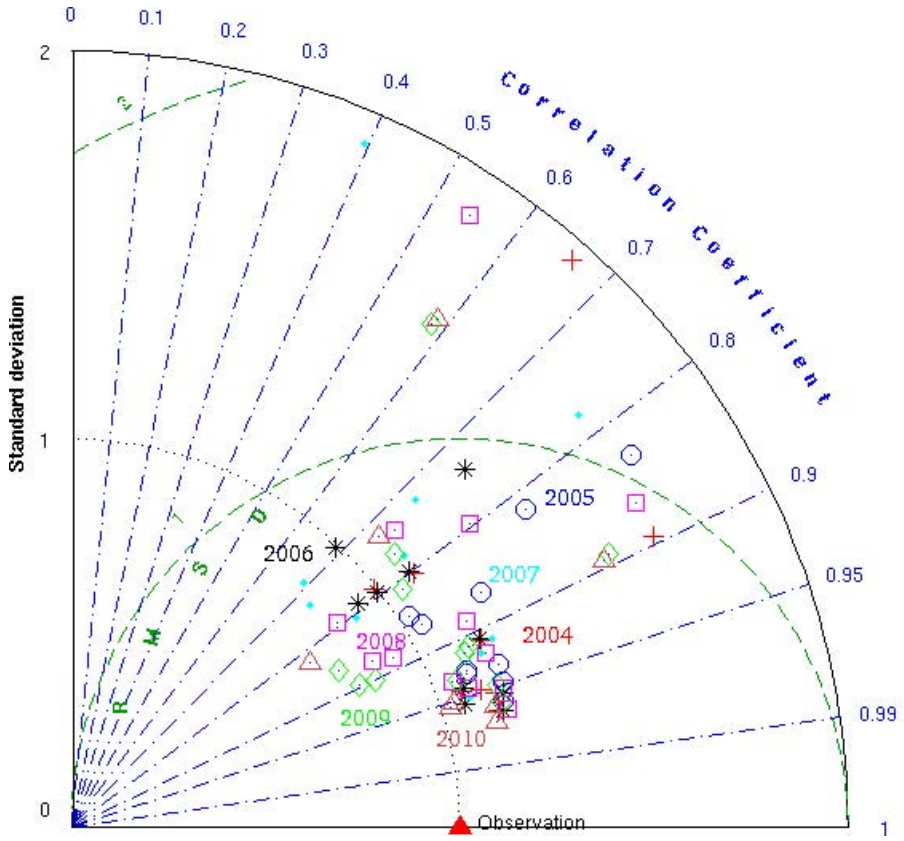

Fig. 4. Taylor Diagram for model simulated and observed sea-level anomaly at 13 tidal stations from 2004 to 2010. Radial distance represents the ratio of simulated to observed standard deviations, and azimuthal angle represents model-data correlation. Green arcs represent centered root mean square difference between model and data.

BGD
10, 7785–7830, 2013

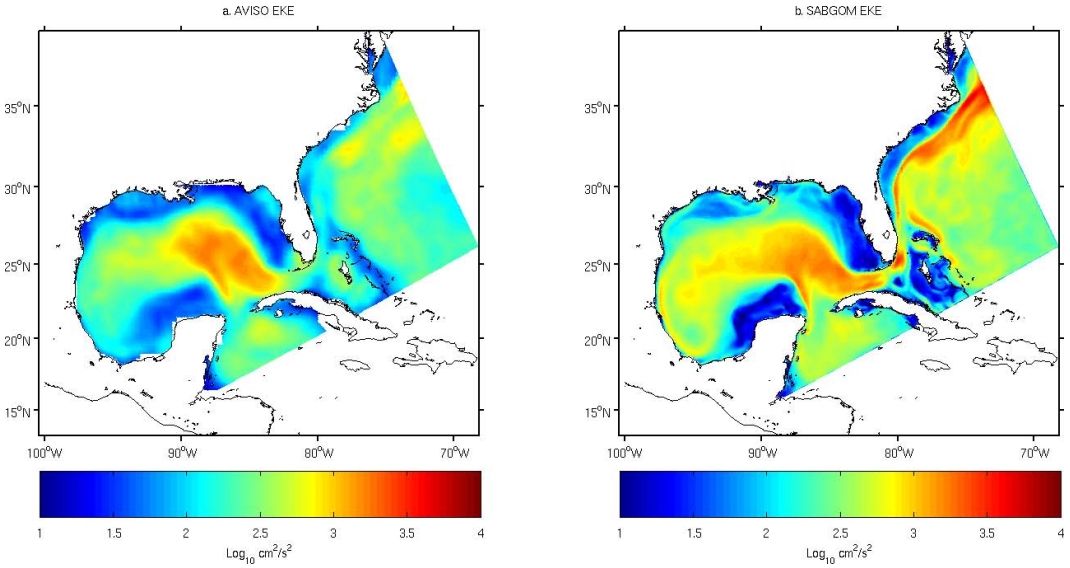

Fig. 5. Comparison of 7 yr (2004–2010) mean eddy kinetic energy calculated based on **(a)** AVISO SSH observation and **(b)** SABGOM model simulated SSH.

BGD
10, 7785–7830, 2013

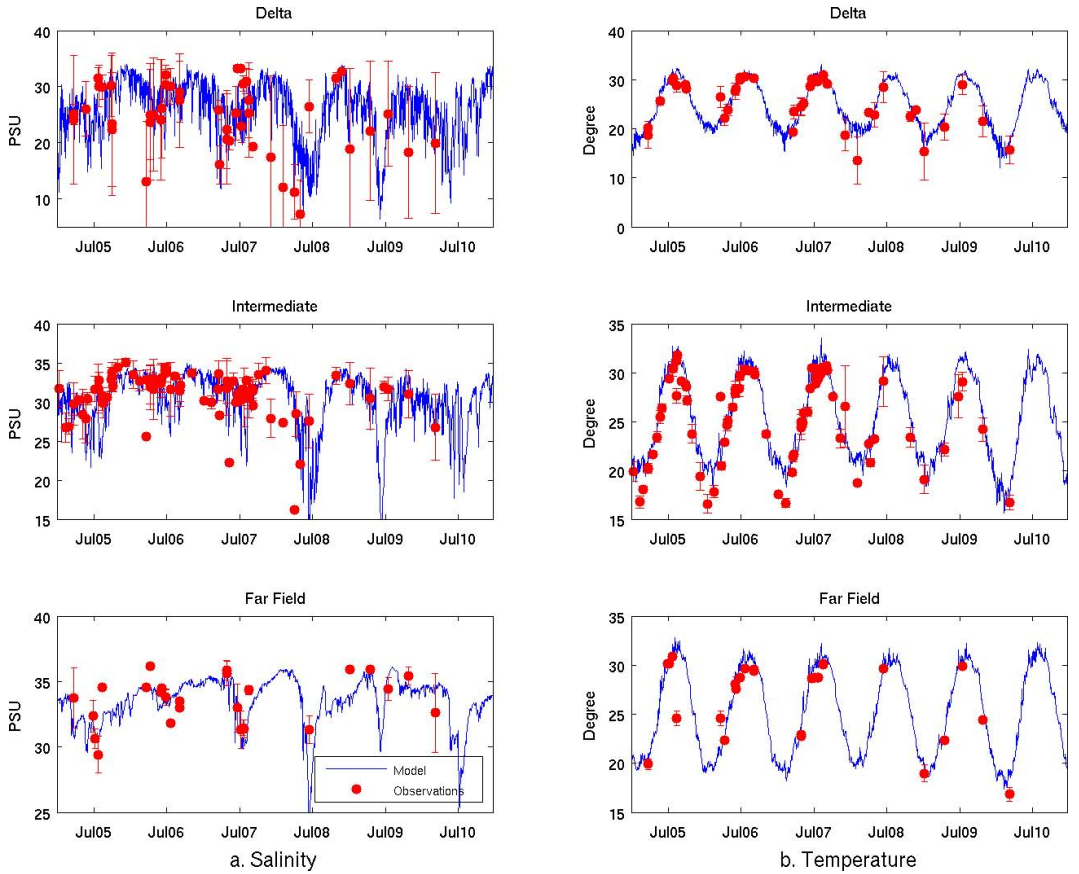

Fig. 6. Time series comparisons between observed and simulated **(a)** sea surface salinity (left panels) and **(b)** sea surface temperature (right panels) in 2005–2010. Results are presented for each of three sub-regions illustrated in Fig. 2. Blue lines are simulated values and filled red circles are observed values. Error bars stand for one standard deviation of available observations.

BGD
10, 7785–7830, 2013

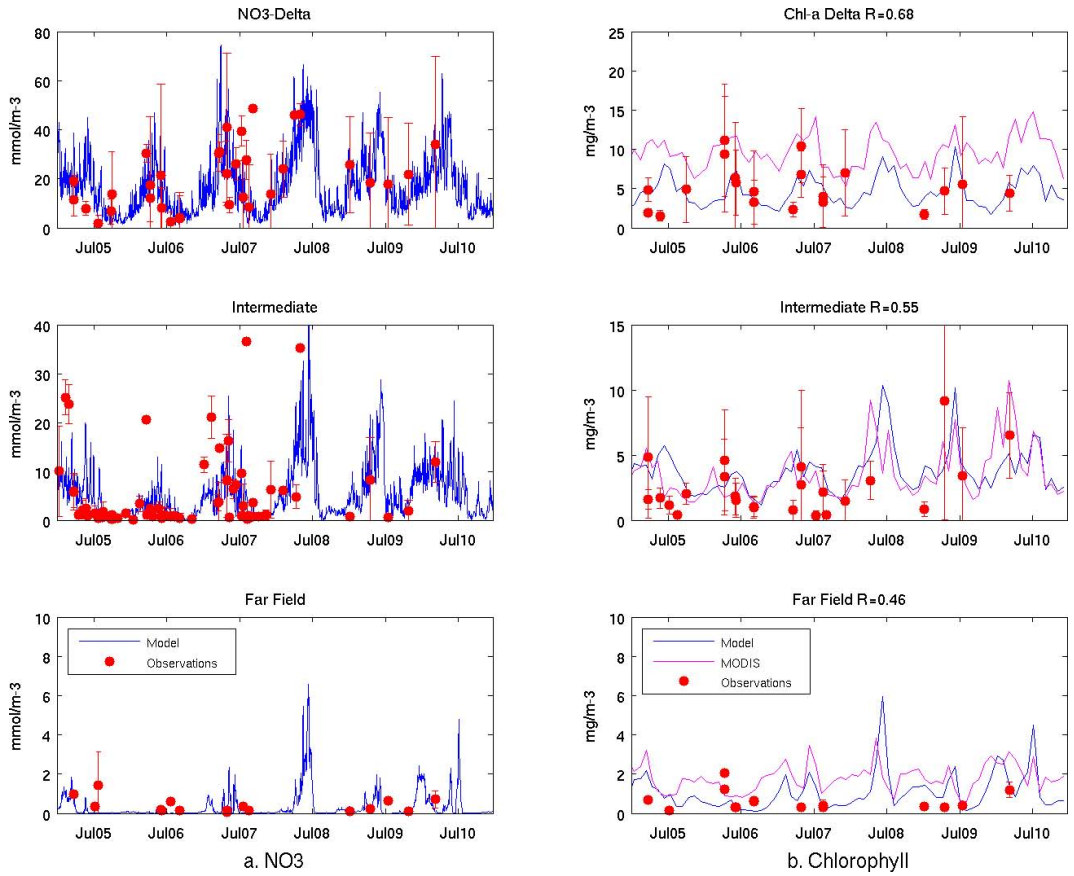

Fig. 7. Time series comparison between observed and simulated (similar to Fig. 6) **(a)** nitrate (left panel) and **(b)** chlorophyll (right panels). For chlorophyll comparison, MODIS monthly mean pigment concentration data (pink line) are also shown for each of three regions.

BGD
10, 7785–7830, 2013

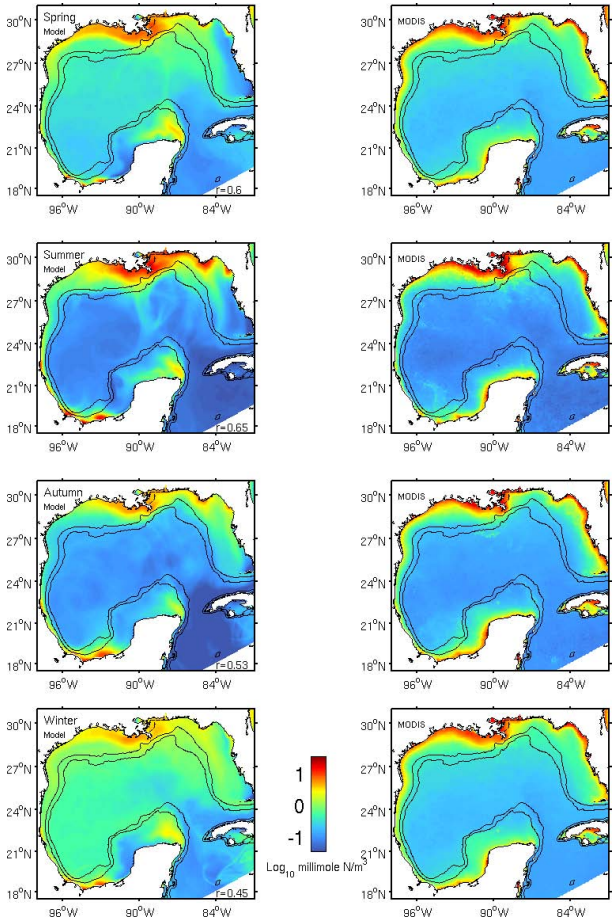

Fig. 8. Comparison of simulated (left panels) and MODIS observed (right panels) seasonal mean surface chlorophyll. Also shown each figure are 200 and 1000 m isobaths.

BGD
10, 7785–7830, 2013

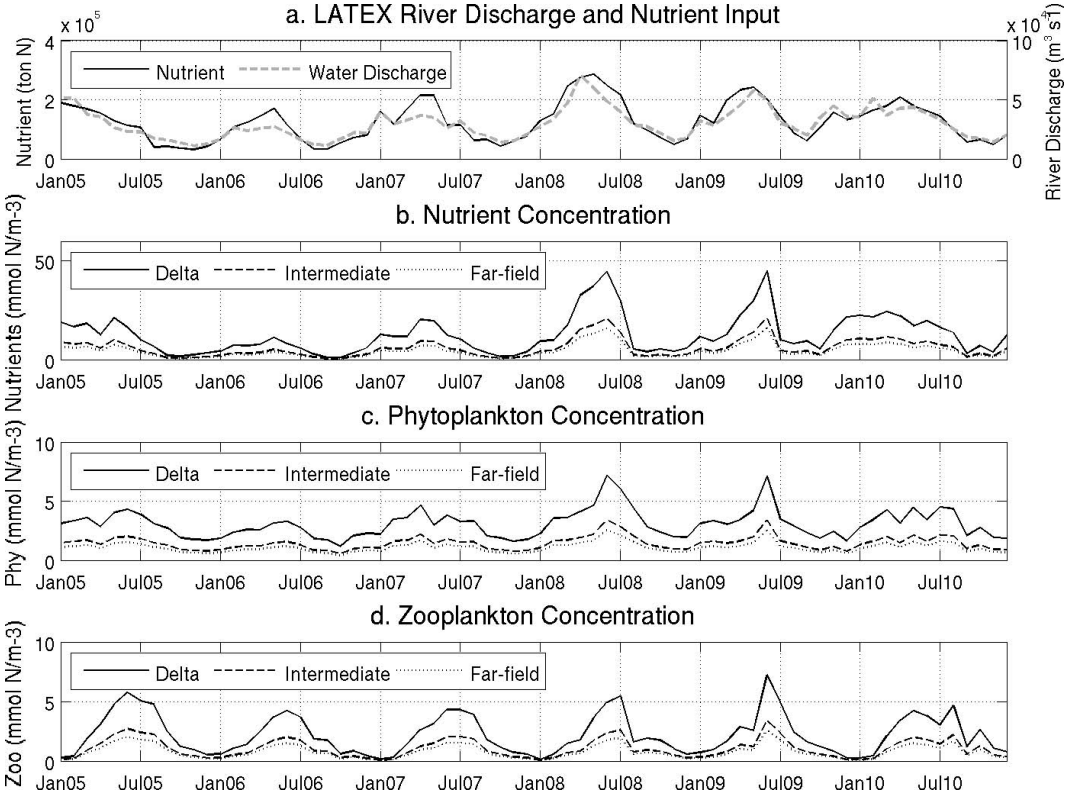

Fig. 9. Monthly mean time series of **(a)** river discharge and nutrient loading, **(b)** surface nutrient concentration, **(c)** surface phytoplankton concentration, and (4) surface zooplankton concentration in each of 3 analysis regions (Delta, Intermediate, Far-field) on the LATEX shelf.

BGD
10, 7785–7830, 2013

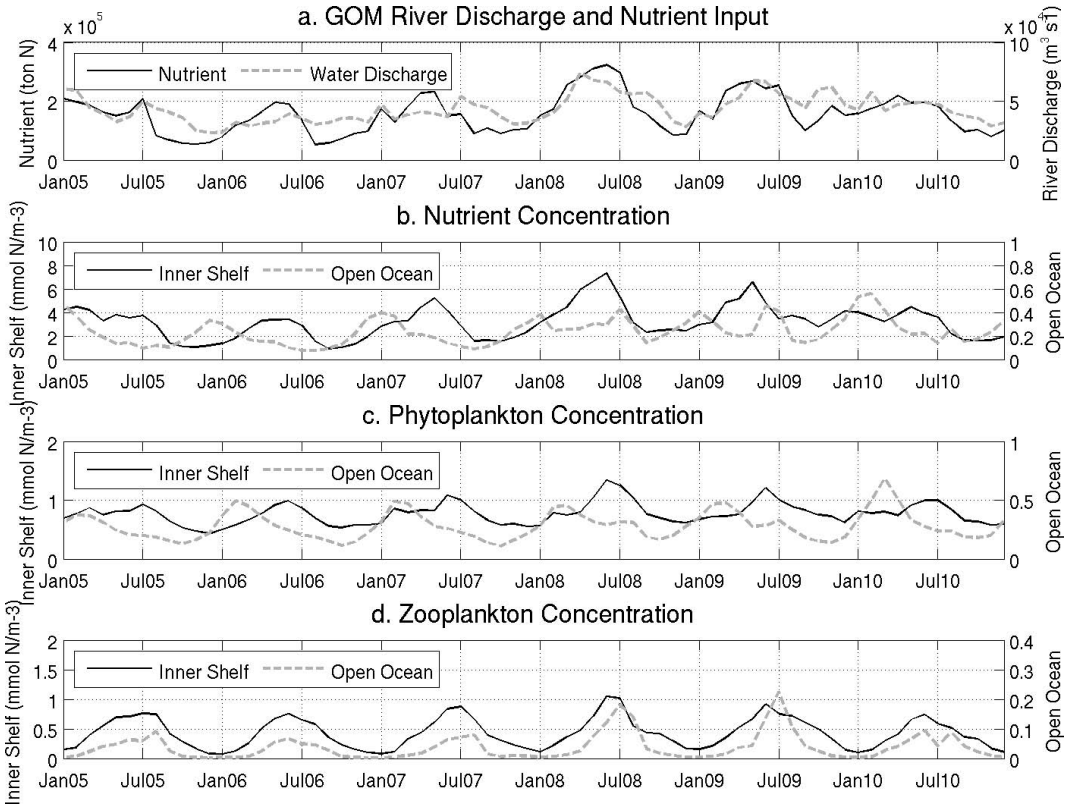

Fig. 10. Monthly mean time series of **(a)** river discharge and nutrient loading, **(b)** surface nutrient concentration, **(c)** surface phytoplankton concentration, and (4) surface zooplankton concentration on the shelf, and deep-sea areas over the entire gulf.

BGD
10, 7785–7830, 2013

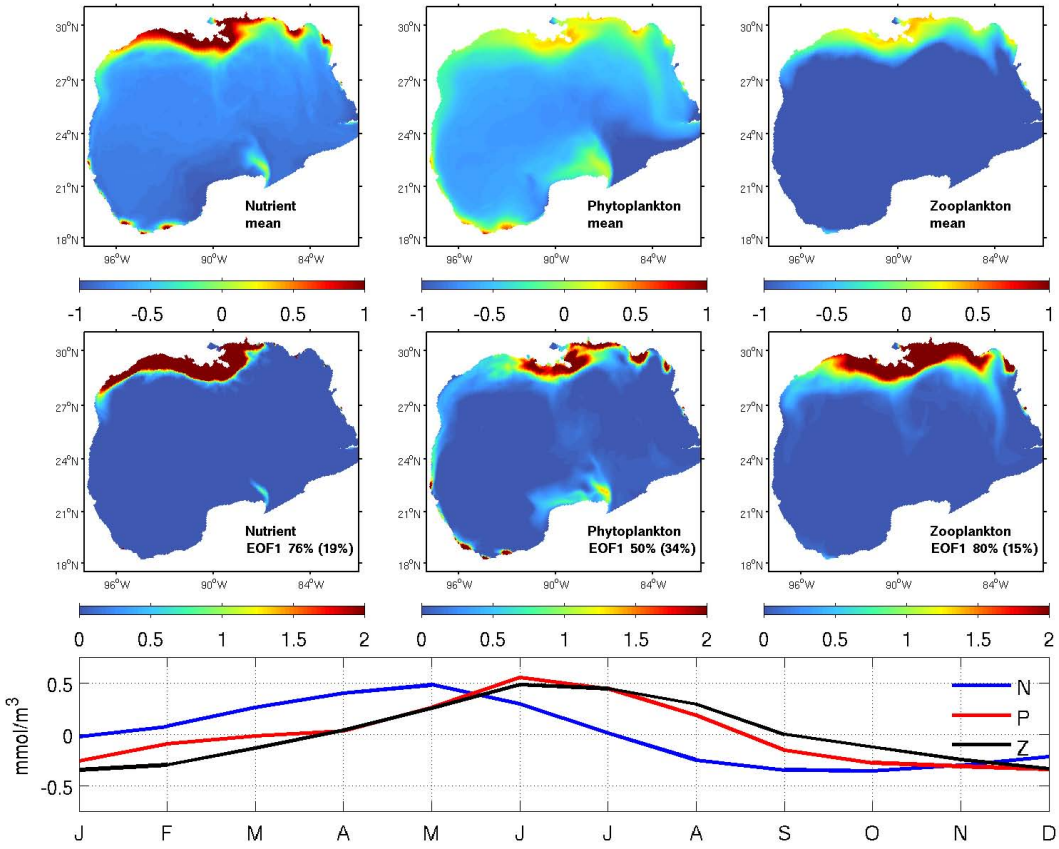

Fig. 11. Empirical Orthogonal Function (EOF) analyses of surface nutrient, phytoplankton and zooplankton fields. Mean fields are shown in the top panels (units: mmol N m^{-3}, log scale), the first EOF modes and the variance they account for are shown in the middle panels and their corresponding 1st principle components are shown in the bottom panels.

BGD
10, 7785–7830, 2013

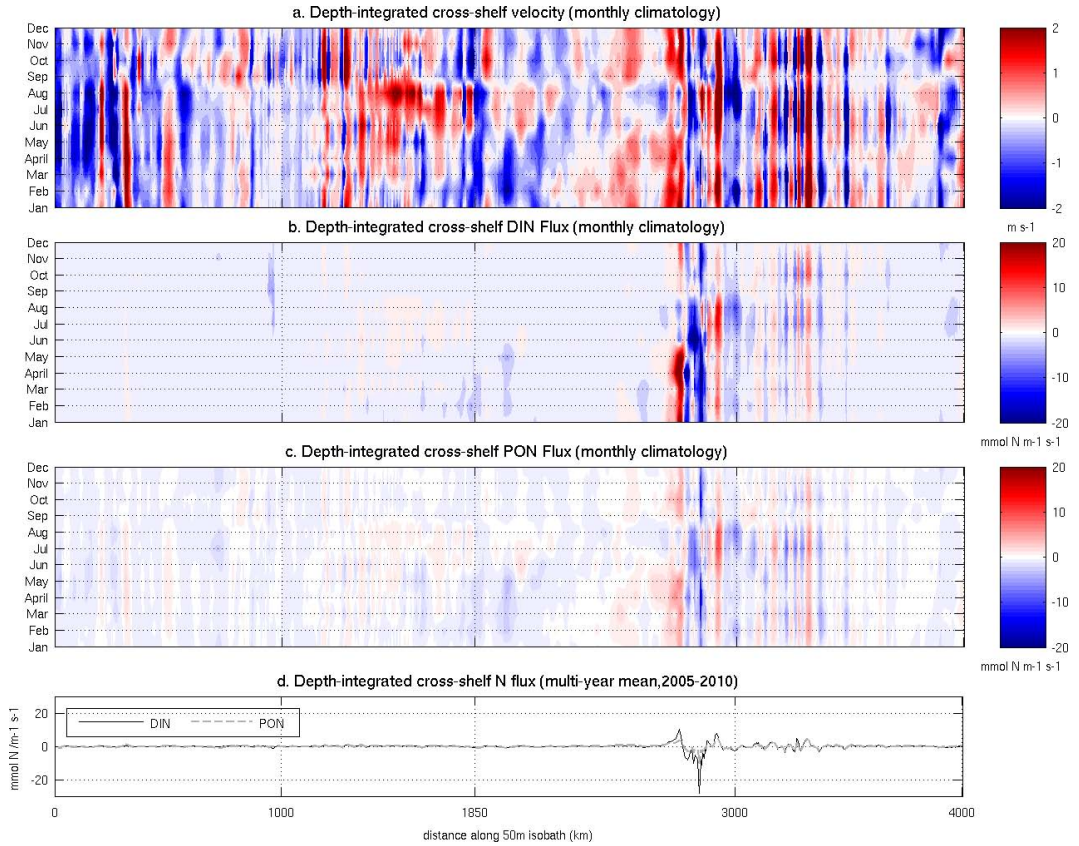

Fig. 12. Depth-integrated monthly mean cross-shelf **(a)** velocity, **(b)** dissolved inorganic nitrogen (DIN) flux, **(c)** particular organic nitrogen (PON) flux and **(d)** annual mean DIN and PON flux cross the 50 m isobath. Positive/negative values stand for shoreward/seaward transport.

BGD
10, 7785–7830, 2013

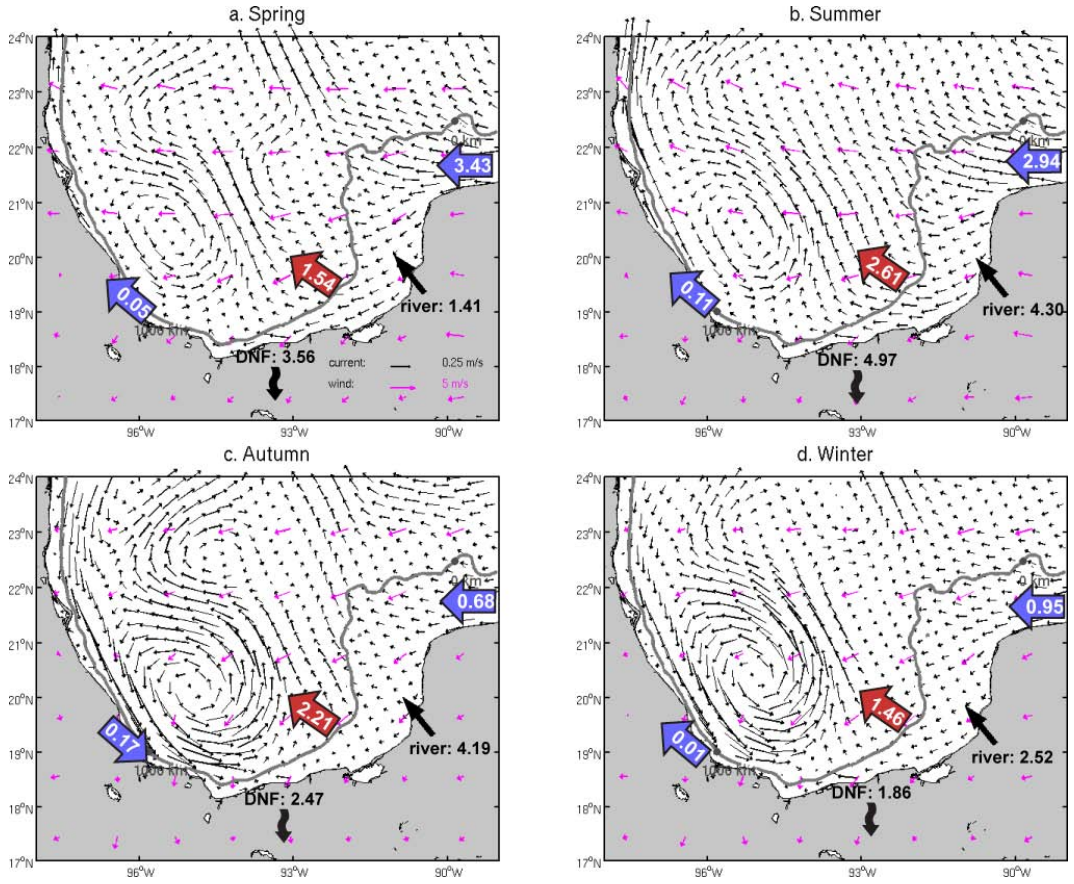

Fig. 13. Seasonal mean surface current and wind fields in the BOC shelf in **(a)** spring, **(b)** summer, **(c)** fall, and **(d)** winter. Also shown is regional along-shelf nutrient flux (blue arrows, unit: 10^9 mol N), cross-shelf nutrient flux (red arrows, unit: 10^9 mol N), river inputs (unit: 10^9 mol N) and denitrification flux (DNF, unit: 10^9 mol N), and 50 m isobath (grey line).

BGD
10, 7785–7830, 2013

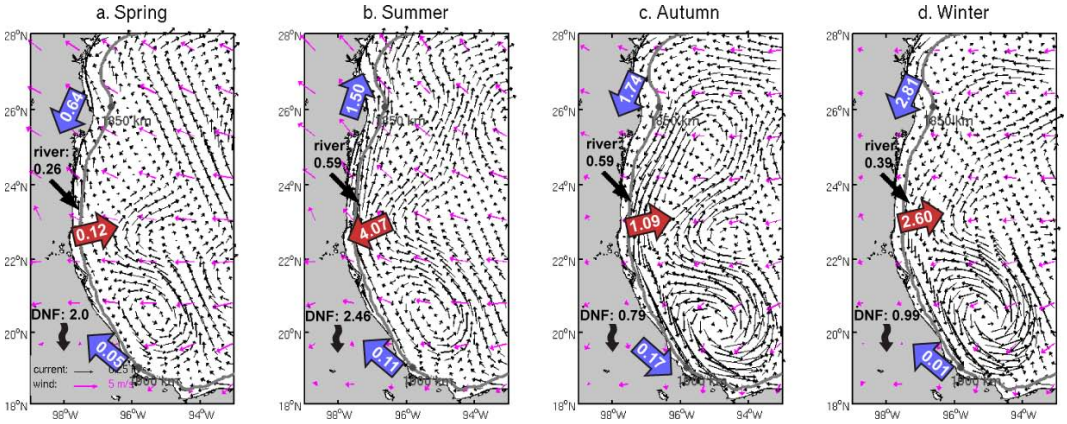

Fig. 14. Similar with Fig. 13 but for the TAVE shelf.

BGD
10, 7785–7830, 2013

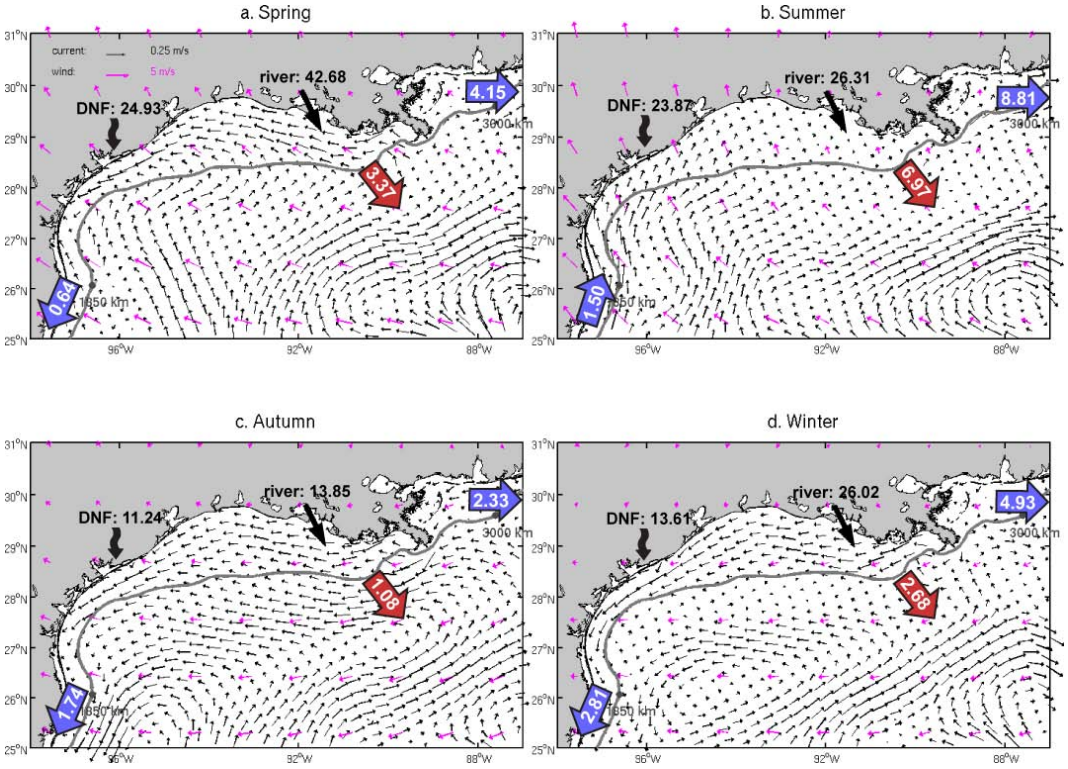

Fig. 15. Similar with Fig. 13 but for the LATEX shelf.

BGD
10, 7785–7830, 2013

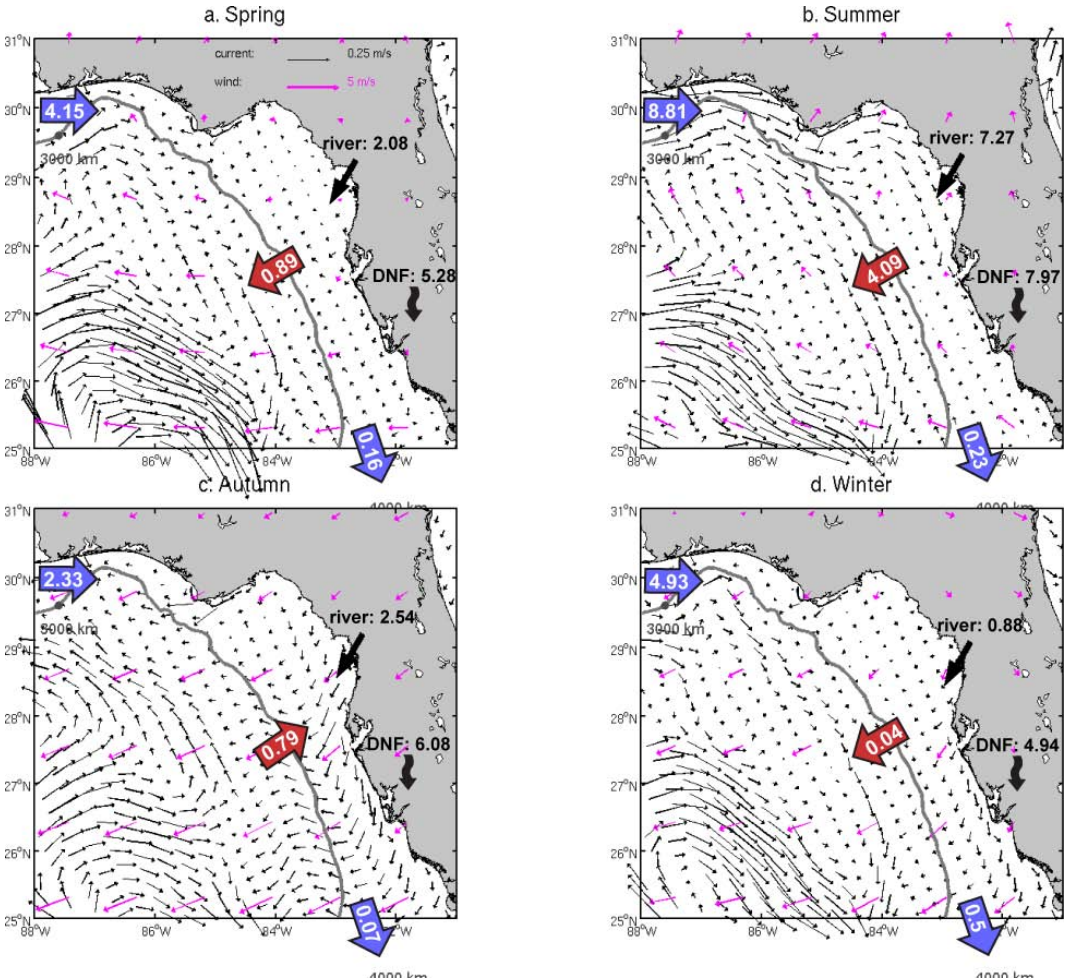

Fig. 16. Similar with Fig. 13 but for the west Florida shelf.

BGD
10, 7785–7830, 2013